Eyster, A., Weiss, B.P., Karlstrom, K., and Macdonald, F.A., 2019, Paleomagnetism of the Chuar Group and evaluation of the late Tonian Laurentian apparent polar wander path with implications for the makeup and breakup of Rodinia: GSA Bulletin, https://doi.org/10.1130/B32012.1.

Data Repository

Supplemental Text

Supplemental Tables

Table DR1. Sampling Locations with Details of Latitude, Longitude, Bedding strike & dip, Formation, and Member

Table DR2. Sample Paleomagnetic results: least squares fits with unblocking ranges

Table DR3. IRM Acquisition Parameters

Table DR4. Backfield And Hysteresis Parameters

Table DR5: HT site component directions from Weil et al. (2004)

Table DR6. Potential Explanation for Walcott Site Means

Table DR7. Reanalyzed A_r data from dated Concajou Canyon sill (Park 1981)

Table DR8. Reanalyzed data from the Hottah Sheets (Park et al. 1995)

Table DR9. Laurentian Paleomagnetic Poles from the Mackenzie Mountains Supergroup

Table DR10. Uinta Mountain Group Paleomagnetic data from Bressler (1981)

Table DR11. Uinta Mountain Group paleomagnetic data Weil et al. (2006)

Table DR12. Select Mesoproterozoic Paleomagnetic Poles

Supplemental Figures

Figure DR1. Rodinia reconstructions for the Western Laurentia margin. A. SWEAT (after Hoffman, 1991; Moores, 1991; and Daizal 1991). B. AUSWUS (after Karlstrom et al., 1999). C. AUSMEX (after Wingate and Giddings, 2000). D. Missing Link China (After Li et al., 2008). E. Missing Link Tarim (After Wen et al., 2016). F. COBRA (after Evans, 2009). G. Siberia (after Sears and Price 1978; 2003). Note that coloring is inconsistent between in order to highlight the different models of the conjugate margin to the western Laurentia margin.

Figure DR2. Paleomagnetic poles from samples that displayed HT components with linear decays to the origin and their overall mean.

Figure DR3. E-I inclination flattening for our Carbon Butte-Awatabi dataset. A. Elongation/inclination pairs as a function of f, data plus 25 bootstrap samples. B. Cumulative distribution of bootstrapped optimal inclinations plus uncertainties. Estimate from original data set plotted as solid line.

Figure DR4. Testing the block rotation of the Colorado plateau by comparing the paleomagnetic poles from the ca. 1094-1080 Ma Grand Canyon Unkar intrusives and Cardenas basalts to the 1095 Ma-1083 Ma portions of the midcontinent rift Logan Loop. A, B, C. Colorado plateau rotated 0, 5, 10° respectively relative to North America using an Euler pole of 34.6°N 254.6°E (Hamilton, 1988).

Figure DR5. (A) Fold test for reanalyzed Carbon Canyon sites (Weil et al., 2004). (B) Elongation/inclination pairs as a function of f, data plus 25 bootstrap samples. C. Cumulative distribution of bootstrapped optimal inclinations plus uncertainties. Estimate from original data set plotted as solid line.

Figure DR6. Uinta Mountain Group poles from Bressler (1981) and Weil et al., (2006). Reported and proposed sampling heights allowed separation of poles into three groupings that were used in subsequent analysis.

Figure DR7. Mackenzie Mountains poles from Park and Jefferson (1991) and references therein.

Figure DR8. Comparison between reconstructions of Congo using both pole polarities. A. Congo in the southern hemisphere. B. Congo in the Northern Hemisphere.

Figure DR9. Comparison between reconstructions of Tarim using the Baiyisi pole (A), as well as both of the less-constrained Qiaoenbrak Formation pole (B).

Figure DR10. ca. 1070 Ma reconstruction with only Laurentia, Australia and associated cratons. Paleomagnetic poles are from the Australian Bangemall sills (1070 Ma U-Pb) and the Laurentian Nonesuch Shale (1087 Ma Re-Os).

Figure DR11. Figures similar to those in the manuscript, but for directions that are corrected for possible inclination flattening.

Previous Rodinia Reconstructions

Early models suggested a Southwest US-East Antarctic (SWEAT) connection based on orogenic piercing points (Moores, 1991) (Fig. S1A) which connected the Grenville orogen of Laurentia to East Antarctica (Dronning Maud Land) and into India and Australia, and connecting the Wopmay orogen of northwest Canada to eastern Australia and into Antarctica (Moores, 1991). In northwest Canada, stratigraphic, metallogenetic, and paleomagnetic data supported the suggestion that northwestern Laurentia and southern Australia were originally connected, but began to rift apart as early as 1200 Ma, and finally began to develop two opposing passive continental margins by about 750 Ma (Young, 1992). In particular, this explained the similar rift history of the two margins: Late Proterozoic rifting and Early Cambrian carbonate platform development (Jefferson, 1978). Hoffman (1991)) expanded on this by suggesting that the rifting centered on Laurentia was followed by fan-like collapse and eventual amalgamation of Gondwana. At the time, paleomagnetic results from Laurentia and Australia seemed to support this scenario, though the dataset was sparse (Powell et al., 1993). Additionally, Daziel (1991) created a Precambrian reconstruction that aligned the Grenville front with a comparable tectonic boundary in East Antarctica truncated along the Weddell Sea margin.

As an alternative, the Australia-SouthWest United States (AUSWUS) model (Fig. S1B) was proposed based on aligning linear rift-transform segments between ancestral Australia and western Laurentia (Brookfield, 1993). It was elaborated by Karlstrom et al. (1999), who showed that the AUSWUS reconstruction was corroborated by similarities in the composition and tectonic setting of Paleoproterozoic-Neoproterozoic rocks between the western U.S. and Australia. Specifically, the presence of juvenile arc assemblages (Yavapai in Laurentia and Arunta in Australia), and quartz arenite-rhyolite sequences (Mazatzal in Laurentia and Reynolds-Musgrave in Australia; Dirks and Wilson, 1990). Finally, both continents contained broadly correlative ore-deposits and, importantly, the southwestern U.S. contained distinctive suites of 1.22-1.07 Ga zircons that required a western source (Ross et al., 1992).

A third hypothesis, the Australia-Mexico (AUSMEX) reconstruction (Fig. S1C) was inspired by paleomagnetic data from the 1.07 Ma Bangemall sills in Australia (Wingate and Giddings, 2004). In addition to satisfying paleomagnetic constraints, this configuration was suggested to align late Mesoproterozoic orogenic belts in northeast Australia and southernmost Laurentia (Wingate and Giddings, 2004), specifically juxtaposing the high-grade metamorphic and magmatic rocks of the Australian Cape River Province with the southern continuation of the Grenville Province of Laurentia (Rivers, 1997).

The Missing Link model (Fig. S1D) initially modified the SWEAT model and suggested that South China was located between Australia—East Antarctica and Laurentia, serving as the ”missing-link” between the two continents (Li et al., 1995). This model resolved some discontinuities in crustal provinces of Australia-East Antarctica and Laurentia, provided a western source region to generate the late Mesoproterozoic detrital grains in the Belt Basin. This model also explained similarities in the Neoproterozoic stratigraphy of South China, southeastern Australia and western Laurentia, and between Cathaysian South China and southern Laurentia. More recently, the Missing Link model has been modified to use the AUSWUS or AUSMEX models for the reconstruction of Australia (Li et al., 2008).

However, there are some recent challenges to this model, in the form of new geochronology and better understanding of the Ediacaran-Paleozoic position of South China (Wen et al., 2016). New

geochronologic data on the assembly of Yangtze and Cathaysia (Sibao or Jiangnan orogen), suggests that orogeny occurred after the Grenville orogeny (Zhao et al., 2011; Wang et al., 2014). Paleomagnetic and geological data indicate that South China likely was adjacent to NW Australia in the early Paleozoic, which requires a complicated path of South China from the missing link position around northern Australia (Li et al., 2013; Cawood et al. 2013). Most recently, some authors have suggested that Tarim may be a more viable missing link (Fig. 1E; Wen et al., 2016). This was suggested in part due to the well-developed Neoproterozoic glacio-rift strata on both continents, as well as similar Paleoproterozoic intrusions (Wen et al., 2016).

West Africa is suggested to be the conjugate craton in the COBRA model (Fig. S1F) that connects ca. 700 Ma rift successions in the North American Cordillera and BRAsiliano-Pharuside orogens (Evans, 2009). This reconstruction with West Africa and Rio de la Plata on the western Laurentian margin is not well constrained paleomagnetically, but is suggested to have existed from 1.8 Ga until the breakup of Rodinia (Evans, 2009).

Finally, the northeastern margin of the Siberian craton has also been proposed to be the conjugate for southwestern Laurentia (Fig. S1G; Sears and Price, 1978, 2003). This was based on matching up Paleoproterozoic to Early Cambrian geology from southwestern Laurentia to the northeastern Siberian craton as well as some paleomagnetic data (Sears and Price, 1978; 2003).

Rotation of the Colorado Plateau

When considering paleomagnetic data, it is important to ensure that the regions are tectonically coherent and have not been complicated by larger regional block rotations. It is suggested that the Laramide orogeny involved a clockwise rotation of about 2-4° of the Colorado Plateau relative to the continental interior (Hamilton, 1988). As the Grand Canyon is located at the very southwest margin of the Colorado plateau, its putative rotation may need to be corrected. Some suggest that the angle of rotation was moderate (5°, Bryan and Gordon, 1990), but more recent paleomagnetic studies have suggested that this clockwise rotation may have been as large as 13.5° to 15° to account for differences in declination of Mesozoic paleomagnetic poles (Kent and Witte, 1993; Steiner and Lucas, 2000; Kent et al., 2012). Luckily, the underlying Cardenas Basalts and Unkar Intrusions can be used to understand the magnitude of the Colorado Plateau rotation in the Grand Canyon area. A normal polarity paleomagnetic pole was obtained from Cardenas Basalts and associated intrusions in the Unkar Group (32°N, 185°E, dp=6.8°/dm=9.3°; n=3 flows, 13 intrusions; Weil et al., 2003). This direction was interpreted to be primary based on a partial contact test of the (Weil et al., 2003). The Cardenas basalt and associated sills and dikes within the Unkar Group were initially dated to 1070±70 Ma (Rb-Sr whole-rock; Elston and McKee, 1982), but subsequently refined to 1103±10 Ma (Ar-Ar contact metamorphic biotite from sill associated with Cardenas basalt; Timmons et al., 2005; reanalyzed by Bright et al., 2014). These volcanics are thought to be the extrusive expression of the southwestern North American diabase province (Hammond, 1990; Howard, 1991; Harlan et al., 1993). Although precise U-Pb ages have not been obtained directly from the Cardenas basalt, the associated diabase intrusions have been dated with U-Pb thermal ionization mass spectrometry (TIMS) at 1080±2 Ma, 1080±3 Ma, 1088±3 Ma, and 1094±2 Ma (Bright et al., 2014). As these units are ca. 1100 Ma that suggests comparison with paleomagnetic results from the Mesoproterozoic (1.1 Ga) Midcontinent Rift (MCR). The U-Pb baddeleyite ages (1080±2 Ma, 1080±3 Ma, 1088±3 Ma, and 1094±2 Ma) obtained by Bright et al. (2014) were used to compare the Unkar Intrusives and Cardenas Basalts with the MCR volcanics (Fig. S4. Table S12).

Early paleomagnetic studies of the MCR, suggested that there might be asymmetric reversals preserved in the volcanics. However, a high-resolution study of paleomagnetic data that spanned three geomagnetic field reversals from a well-described series of basalt flows at Mamainse Point showed that each reversal was in fact symmetric and the previously documented reversal asymmetry was an artifact of the rapid motion of North America during this time (Swanson Hysell, et al., 2009). Now the Keweenaw volcanics provide one of the best constrained geochronologic and paleomagnetic parts of the Precambrian Laurentian APWP. Given the age constraints, the Chengwatana Volcanics (1094.6±2.1 Pb-Pb Zartman et al., 1997), Schroeder-Lutsen Basalts (<1091.61±0.14 Ma chemical abrasion-isotope dilution-thermal ionization mass spectrometry [CA-ID-TIMS] Fairchild et al., 2017), the Lake Shore Traps (1085.57±0.25 Ma CA-ID-TIMS Fairchild et al., 2017), and the Michipicoten Island Formation (1084.35±0.20 Ma and 1083.52±0.23 CA-ID-TIMS Fairchild et al., 2017) are of particular relevance for this study.

The suggested rotation of the Colorado plateau with a pole at 34.6°N 254.6°E (Hamilton, 1988) was applied for three different cases: rotations of 0°, 5°, and 10° of the Colorado plateau and associated pole (Fig. S3). In the unrotated state, the Cardenas-Unkar Intrusive pole lies coincident with the Chengwatana Volcanics. When the Colorado plateau is rotated greater than 15 degrees, the A_{95} of the Cardenas-Unkar Intrusive pole no longer overlaps with any of the Keweenawan volcanics. The uncertain age constraints on the Cardenas-Unkar Intrusive pole hinders a robust comparison. However, the data suggest that the Colorado plateau has rotated less than 15°, most likely less than 5°, and is most similar to the Keweenawan poles in its unrotated state. Thus corrections for large-scale tectonic block rotations were not applied.

Expanded discussion of previous paleomagnetic data from the Chuar Group

The Chuar Group has been the focus of several paleomagnetic studies but much of the initial work was never published in peer-reviewed journals, instead only summarized in abstracts or review papers with no demagnetization or sample data (Elston, 1989; Elston, 1986; Link et al., 1993). The only previous published demagnetization and sample data from the Chuar Group is from a study conducted by Weil et al. (2004) that focused on the Kwagunt and Galeros formations (Table S5). From the Galeros formation, the Jupiter and Carbon Canyon members were sampled and resolvable shallow to intermediate directions were obtained with unblocking temperatures of 630-680°C (indicative of hematite). As there were only two sites from the Jupiter member, they were combined with the sites from the Carbon Canyon member, and these combined directions passed the fold test (Weil et al., 2004). From the Kwagunt Formation, samples were collected from the Carbon Butte, Awatabi, and Walcott members. Most of the Kwagunt samples had discrete low inclination, E-W trending directions with unblocking temperatures between 650 and 680°C (as expected for hematite) (Weil et al., 2004). For some samples, there was also a north-directed, moderate-steep positive inclination magnetization overprint removed upon heating to 300°C and interpreted as a recent overprint (Weil et al., 2004). However, for nine sites from the Carbon Butte Member this component displayed unblocking temperatures up to 680°C (Weil et al., 2004). For the combined Kwagunt members, a fold test was applied (Tauxe, 1998), resulting in maximum clustering at 80% unfolding and was interpreted to support a primary magnetization acquired at the time of, or soon after, deposition (Weil et al., 2004).

Additional information on paleomagnetic data for other cratons

<u>Australia</u>

Rift basins in Australia are interpreted to represent two episodes of extension, one ca. 700-650 Ma the second ca. 600 Ma, with extension suggested to be off the present day eastern margin (Preiss et al., 1978; Walter et al., 1995; Preiss, 2000 Greene, 2010). Some have suggested that rifting was associated with ca. 825-750 Ma mafic dikes and volcanism (Wingate and Giddings, 2000; Li et al., 1999; Ernst et al., 2008). Focus on the southern Georgina Basin has suggested that the Neoproterozoic continental margin of Australia consisted of northwest striking rift segments offset by northeast striking transform faults (Greene, 2010); however, this interpretation is not unique and focuses on sedimentation that post-dates 780-720 tectonism.

Mundine Dike Swarm Pole

An extensive swarm of dolerite dikes, the Mundine Dike Swarm, intrude into Archean and Proterozoic rocks of the Pilbara Craton of Western Australia. Most of the dikes are less than 30 meters wide and are fine- to medium-grained, although some are wider, coarse-grained, and have individual strike lengths of over 200 km (Wingate and Giddings, 2000). A joint geochronologic and paleomagnetic study obtained Pb-Pb zircon data and a paleomagnetic pole that placed Australia at low latitudes.

Zircons grains were isolated from the center of a medium- to coarse-grained 25-meter wide quartz dolerite dike (Wingate and Giddings, 2000). From the various SHRIMP analyses the Pb-Pb ages all agreed within error, but when considering $^{206}Pb/^{238}U$ ratios, two analyses were slightly normally discordant and more than half were strongly reversely discordant (Wingate and Giddings, 2000). This suggested unsupported radiogenic Pb (Mattinson et al., 1996), or enhanced sputtering of Pb relative to U, due to radiation-induced microstructural changes (McLaren et al., 1994). Thus the reported age is from a weighted mean Pb-Pb age of 755±3 Ma. The paleomagnetic study obtained a positive baked contact test to indicate that the magnetization from the Mundine Dike Swarm was from emplacement and cooling at 755 Ma (Wingate and Giddings, 2000). This paleomagnetic data for eight dikes was combined with the previous results for six Northampton dikes to obtain the paleomagnetic pole for Australia at 750 Ma (Wingate and Giddings, 2000).

Walsh Tillite Cap

The Wash Tillite is a glacial diamictite exposed in eastern Kimberley, northwestern Australia. Initially, researchers suggested that the Wash Tillite might be correlative with the Sturtian deposits (Dow and Gemuts, 1969; Plumb and Gemuts, 1976). However, more recent work has suggested that the Wash Tillite should be correlative with the younger Marinoan glacial deposits (Plumb, 1981; Grey and Corkeron, 1998; Coats and Preiss, 1980). A paleomagnetic study sampled the cap carbonate overlying the Wash Tillite (the Wash Tillite Cap-WTC) and obtained a direction from six sites that passed a fold test (Li, 2000). As the resulting paleomagnetic pole was 58° away from the Elatina Formation pole expected for the Marinoan glaciation, this led to the suggestion that the Walsh Tillite was Sturtian (ca. 770-750 Ma) rather than Marinoan in age, and the WTC pole was introduced as a ca. 750 tie point for Australia in reconstructions (Maloof et al., 2006; Li et al., 2008; Zhang et al., 2006; Li and Evans, 2011). When incorporated into paleogeographic reconstructions, it was used to argue for the break-up of Rodinia by 750 Ma. However, the dismissal of the geological correlations in favor an arbitrary 750 Ma age is puzzling, and given recent geochronological calibrations on Snowball Earth glaciations, the likely age for the WTC pole is either 662 Ma (if a Sturtian cap), or more likely 632 Ma (a Marinoan cap) (Rooney et al., 2015). With these revised age constraints, this paleomagnetic pole was not used in the presented reconstructions.

Yilgarn Dikes

The paleomagnetic pole from the Yilgarn B dikes of Western Australia was initially thought to be robust and used as a tie point for all 1050-700 Ma reconstructions (Giddings, 1976). This pole was one of the original paleomagnetic constraints for the SWEAT hypothesis (Powell et al., 1993). However, a paleomagnetic study resampled the same rocks from which a positive baked contact test was reported, but obtained a negative baked contact test (Halls and Wingate, 2001). This was combined with petrographic and rock magnetic data to suggest that that pole was a secondary overprint likely Mesozoic in age (Halls and Wingate, 2001). Thus, this pole was not used in the presented reconstructions.

South China

South China comprises the Yangtze and Cathaysia blocks (Grabau, 1924). The Yangtze block has a late Archean–Paleoproterozoic core and younger orogenic belts (Wang et al., 1995), while the Cathaysia block has pre–1.4 Ga continental crust (Jahn et al., 1990; Li et al., 1992; Shui, 1987; Zhou et al., 1993; Li, 1994). There are well-developed Neoproterozoic rift systems in South China, that have helped served as a geologic basis for proposed connections to Australia and Laurentia (Wang, 1985; Xing, 1989; Qiao, 1989a, 1989b; Dong and Liu, 1991; Li, 1991; Li et al., 1995).

Liantuo Formation

Exposed in the Hubei province and the lower Three Gorges of the Yangtze River, the arkosic to argillitic Liantuo Formation contains interbedded volcanic ash horizons, and is laterally equivalent to the Tonian Banxi Group. Unconformably overlying the Liantuo Formation is the Marinoan Nantuo Formation (Wang et al., 1981; Liao, 1981; Condon et al., 2005). These units have been suggested to reflect continent rifting and passive-margin development, similar in style and age to those found in Australia and western Laurentia. This observation helped place it as a missing link between Australia and Laurentia (Li et al., 1995; Li et al., 1996; Li et al., 2008). However, other work suggests that South China is surrounded by a 970-750 Ma arc, explaining the abundant ash interbeds within the Banxi Group and Liantuo formation (Cawood et al., 2013). Consistent with this alternative interpretation, some have placed it near the northwest Australian shelf (Kirschvink, 1992; Cawood et al., 2013).

North China

The North China Block has an Archean to Paleoproterozoic basement, and Meso-Neoproterozoic to sedimentary basins (e.g. Wang and Qiao, 1984). Some reconstructions place North China near Siberia (Li et al., 1996), while others have suggested that North China was alongside western Laurentia (Wang et al., 1997). Unfortunately, there is sparse paleomagnetic data for North China, and the Nanfen Pole has been used to suggest that North China was connected to Laurentia and near Siberia until 700 Ma (Zhang et al., 2006). Unfortunately, the sample and demagnetization data from the Nanfen pole has not been published in peer-reviewed literature (Lin, 1984) and the age of the Nanfen Formation is unknown. Newer work correlates the Nanfen Formation with the lower part of the ca. 890-925 Ma Huaibei Group (e.g. Xiao et al., 2014). Thus, this paleomagnetic pole was not incorporated into the presented reconstructions. The newer correlations suggest that there are no Cryogenian-Ediacaran basins that could be tie points to the margin of Laurentia. As Mesoproterozoic work has suggested that North China was near Siberia (Zhang et al., 2006; Fu et al., 2015), North China is tenuously placed close to Laurentia and Siberia but this reconstruction lacks constraints.

Tarim

Tarim's basement is composed of Proterozoic schist of the Aksu Group that is intruded by a series of

unmetamorphosed northwest-trending mafic dikes. The overlying sedimentary sequences consist of the Cryogenian Baiysi, Qiaoenbrak and Yuermeinak Formations, and the Ediacaran Sugetbrak and Chigebrak Formations (Gao et al., 1985; 1993; Turner, 2010; Zhu et al., 2011; Xu et al., 2013; Wen et al., 2015). Both the Qiaoenbrak and Yuermeinak Formations are dominated by sandstone, siltstone and conglomerate, and contain diamictites interpreted to record multiple Cryogenian glaciations (Gao et al., 1985; Gao and Qian, 1985; Wen et al., 2015). Marinoan-age cap dolostone was recently documented above the glacial deposits of the younger Yuermeinak Formation (Wen et al., 2015). It is suggested that Tarim was adjacent to northwest Australia (Li et al., 1996; Li et al., 2008), next to Laurentia as a missing link alternative (Wen et al., 2015), or near North China (Wang et al., 2015).

North Australia

North Australia is suggested to have been close to West Australia during the Neoproterozoic, but experienced a later relative rotation (Schmidt et al., 2006; Li and Evans, 2011).

India

The earliest proposed models of Rodinia suggested that East Gondwanaland (India-Australia-Antarctica) remained intact during the tenure of the supercontinent (Hoffman, 1991). However, evolving paleomagnetic data suggests that this may not have been the case (Torsvik et al., 2001b, 2001c; Gregory et al., 2009; Meert et al., 2013).

Malani igneous suite

The extensive felsic Malani igneous suite in northwest India includes an initial phase of felsic extrusives over 3 km thick, followed by intrusion of granite plutons. The final stage includes crosscutting rhyolitic dikes (Mukherjee, 1966; Bhushan, 1985). The unmetamorphosed igneous suite was folded prior to the deposition of overlying sediments (Mukherjee, 1966; Bhushan, 1985).

U-Pb zircon ages of 751±3 and 771±2 Ma were reported in the paleomagnetic study of Torsvik et al. (2001b) as personal communication from R. D. Tucker. Subsequently, a U-Pb secondary ion mass spectrometry (SIMS) 771±5 Ma (MSWD = 1.5) age was obtained from 14 concordant analyses on 10 zircon crystals from a rhyolitic tuff (Gregory et al., 2009). More recently, LA-ICP-MS discordant analyses on zircon from a mafic dike resulted in U-Pb dates ranging between 700 to 727 Ma (weighted mean U-Pb ca. 704 Ma, Pb-Pb 752±18 Ma) (Meert et al., 2013).

Several studies have examined the Malani igneous suite, from which a grand mean pole has been reported (Torsvik et al., 2001b, Gregory et al., 2009; Meert et al. 2013). The primary nature of the pole is supported by baked contact tests and a statistically positive fold test (Torsvik et al., 2001b; Gregory et al., 2009; Meert et al., 2013). This data suggests that India was at intermediate latitudes and likely not part of East Gondwana.

Mahe intrusives- Seychelles

Although a continental fragment, the Seychelles has been placed adjacent to India until around 65 Ma (Plummer and Belle, 1995; Torsvik et al., 1998). The Mahe intrusives of the Seychelles include granite intrusions as well as basaltic and dolerite dikes. TIMs work was conducted on zircon from the Takamaka dolerite dyke, resulting in a U-Pb age of 750.2±2.5 (Torsvik et al., 2001). Following AF and thermal demagnetization, paleomagnetic results from 7 dikes suggested that a primary direction was carried by magnetite or titanium-poor titanomagnetite (Torsvik et al., 2001c). This direction was

supported by 4 of the 7 van der Voo criteria (lack of tectonic coherence with the India craton and no field tests or reversals) (Torsvik et al., 2001c). The Seychelles was then restored relative to India and the Malani intrusive suite (Euler pole: Latitude=25.8°, Longitude=330° and rotation angle=28°) (Torsvik et al., 2001c). However, as this restoration relied on paleomagnetism and the assumed coeval nature of the Malani intrusive suite and the Mahe Intrusives rather than a geologic basis, only the Malani intrusive suite pole was used to constrain India in the reconstructions presented here.

Antarctica, Baltica, Amazonia, Kalahari, Rio de La Plata, Sao Francisco, West Africa

There is no paleomagnetic data for Antarctica, Baltica, Amazonia, Kalahari, Rio de La Plata, Sao Francisco, and West Africa during the 780-720 Ma period, other published configurations were examined before these cratons were incorporated into the reconstructions presented here (Hoffman, 1991; Li et al., 2008; Evans, 2009; Li and Evans, 2011, Li et al., 2013; Merdith et al., 2017).

Antarctica is placed in connection to Australia in its Gondwana configuration (Harley, 2013). The original SWEAT model suggested that eastern Antarctica was connected in its Gondwana configuration with Australia and India, and lay adjacent to the southwestern United States. Subsequent work has identified features related to a Pinjarra Orogen suggesting that eastern Antarctica should be split into an eastern Antarctic craton and the Mawson craton, the latter suggested to be connected to Australia as a single craton post 1200 Ma (Fitzsimons, 2003a, b; Cawood and Buchan 2007; Cawood & Korsch 2008; White et al. 1999). This treatment of the Mawson craton was incorporated into the presented reconstructions.

For Baltica, the Sveconorwegian Orogen is a geologic tie point to the Laurentian Grenville Orogen, and thus most reconstructions place Baltica adjacent to the northeastern margin of Laurentia, although the exact configuration is uncertain (Hoffman, 1991; Bogdanova et al., 2008; Evans, 2009). Similarly, the Amazonian Rondonia-Sunsas orogenic belt may be correlative with the Grenville Orogen, suggesting that Amazonia also be placed adjacent to the Laurentian eastern margin (Hoffman, 1991; Loewy et al., 2003; Davidson, 2008; Li et al., 2008). Further south, the Grenville aged Namaqua-Natal orogenic of the Kalahari Craton was suggested as a tie point to southeast Laurentia (see Hoffman, 1991; Li et al., 2008). There are also proposed connections between Kalahari, Rio de la Plata and Laurentia, so Rio de la Plata is placed adjacent to the eastern margin of Laurentia between Kalahari and Amazonia (Li et al., 2008; Evans, 2009). Another smaller craton, Sao Francisco is placed farther from Laurentia's margin, but adjacent to the Congo (Li et al., 2008; Evans, 2009).

In considering West Africa, there are very few constraints, either geological or paleomagnetic. The craton lacks Grenville aged metamorphism and so it was either part of a larger craton such as Amazonia, or not part of the supercontinent (Trompette, 1997; Merdith et al., 2017). Recent reconstructions were followed by placing West Africa near Amazonia (Merdith et al., 2017).

Long-lived AUSMEX-like configuration?

The possible configuration for Australia and Laurentia at ca. 1070 Ma is also restored (Fig. S8; Table S12) based on the Australian Mesoproterozoic Bangemall sills and the more recently dated Laurentia Nonesuch Formation (Wingate et al. 2002; Cumming et al., 2010). Exposed in the Mesoproterozoic Bangemall basin, the dolerite Bangemall sills intrude into unmetamorphosed, fine-grained carbonate and

siliciclastic marine sedimentary rocks known as the Bangemall Supergroup (Muhling and Brakel, 1985; Martin et al., 1999). The southern parts of the basin were subsequently folded as part of the Edmund Fold Belt (Muhling and Brakel, 1985). Geochronology work on baddeleyite and zircon yielded ages of 1071±8, 1067±14 and 1068±22 Ma, which were combined to yield a mean age of 1070±6 Ma (Wingate et al. 2002). The paleomagnetic direction from the Bangemall Sills has been tilt corrected and is supported by a partial baked contact test, in that the baked rocks had overprint, but no stable direction was obtained from the unbaked host rocks (Wingate et al. 2002; Wingate and Giddings, 2000).

This Bangemall pole is compared with paleomagnetic data from the Laurentian midcontinent rift. The Nonesuch Formation consists of gray-to-black siltstones, shales and very fine sandstone deposited in anoxic water. Recent work has been done using Re-Os geochronology to obtain an age of 1078 ± 24 Ma for the Nonesuch Formation (Cumming et al., 2010). Although the overlying Freda Formation lacks direct geochronologic constraints, it alternatively might be a more correct temporal comparison (Swanson-Hysell et al. 2012; Fairchild et al. 2017). These new age constraints still support a ca. 1070 Ma AUSMEX configuration for Australia and Laurentia (Wingate et al., 2002).

Additional References

Aitken, J. D., 1993, Tectonic evolution and basin history. In: Sedimentary Cover of the North American Craton in Canada. D.E. Stott and J.D. Aitken, (eds.): Geological Survey of Canada, Geology of Canada, no. 5, p. 483−504.

Alt, J. C., 1999, Very low-grade hydrothermal metamorphism of basic igneous rocks, in Low-Grade Metamorphism, edited by M. Frey and D. Robinson, p. 169 – 201, Blackwell, Malden, Mass.

Alt, J. C., and D. A. H. Teagle, 2003, Hydrothermal alteration of upper oceanic crust formed at a fast-spreading ridge: Mineral, chemical and isotopic evidence from ODP Site 801, Chem. Geol., 201, 191–211.

Balgord, E.A., Yonkee, W.A., Link, P.K. and Fanning, C.M., 2013, Stratigraphic, geochronologic, and geochemical record of the Cryogenian Perry Canyon Formation, northern Utah: Implications for Rodinia rifting and snowball Earth glaciation: Geological Society of America Bulletin, v. 125, no. 9-10, p.1442-1467.

Books, K. Magnetization of the lower most Keweenawan lava flows in the Lake Superior area, Geological Survey research 1968, chapter D. U.S. Geological Survey Professional Paper P 0600-D, 248–254 (1968).

Bowring, S.A., Schoene, B., Crowley, J.L., Ramezani, J. and Condon, D.J., 2006, High-precision U-Pb zircon geochronology and the stratigraphic record: Progress and promise. Paleontological Society Papers, v. 12, p. 25.

Brady, P. V., and S. R. Gislason. 1997, Seafloor weathering controls on atmospheric CO2 and global climate: Geochim. Cosmochim. Acta, 61, 965–973.

Brett, J.S. and Dunlop, D.J., 2008. Earth and Planetary Science Letters, 266(1), p.125-139.

Bright, R.M., Amato, J.M., Denyszyn, S.W. and Ernst, R.E., 2014. U-Pb geochronology of 1.1 Ga diabase in the southwestern United States: Testing models for the origin of a post-Grenville large igneous province. Lithosphere, pp.L335-1.

Brock, A., 1968, Metasomatic and intrusive nepheline-bearing rocks from the Mbozi syenite-gabbro complex, southwestern Tanzania. Can. J. EarthSci., v. 5, p. 387-419.
Bryan, P. and Gordon, R.G., 1990. Rotation of the Colorado Plateau: An updated analysis of paleomagnetic poles. Geophysical Research Letters, 17(10), pp.1501-1504.
Buchan, K. L., and Ernst, R. E., 2013, Diabase dyke swarms of Nunavut, Northwest Territories and Yukon, Canada: Geological Survey of Canada, Open File 7464, 24 p.
Calver, C.R., Crowley, J.L., Wingate, M.T.D., Evans, D.A.D., Raub, T.D. and Schmitz, M.D., 2013, Globally synchronous Marinoan deglaciation indicated by U-Pb geochronology of the Cottons Breccia, Tasmania, Australia: Geology, v. 41, no. 10, p.1127-1130.
Cawood, P.A., Wang, Y., Xu, Y. and Zhao, G., 2013. Locating South China in Rodinia and Gondwana: A fragment of greater India lithosphere?. Geology, 41(8), pp.903-906.
Christie-Blick, N., and Levy, M., 1989, Concepts of sequence stratigraphy, with examples from strata of late Proterozoic and Cambrian age in the western United States, in Christie-Blick, N., and Levy, M., eds., Late Proterozoic and Cambrian Tectonics, Sedimentation and Record of Metazoan Radiation in the Western United States (28th International Geological Congress FieldTrip Guidebook T331): Washington, D.C., American Geophysical Union, p. 23–37.
Christie-Blick, Nicholas, 1997, Neoproterozoic Sedimentation and Tectonics in West-Central Utah [Ph.D. Thesis]: Brigham Young University Geology Studies, 30 p.
Fahrig, W. F., and Schwarz, E. J., 1973, Additional paleomagnetic data on the Baffin diabase dikes and a revised Franklin pole, Canadian Journal of Earth Sciences, v. 10, no. 4, p. 576-581.
Fahrig, W. F., Irving, E., and Jackson, G. D., 1971, Paleomagnetism of the Franklin diabases: Canadian Journal of Earth Sciences, v. 8, no. 4, p. 455-467.
Fairchild, L.M., Swanson-Hysell, N.L., Ramezani, J., Sprain, C.J. and Bowring, S.A., 2017, The end of Midcontinent Rift magmatism and the paleogeography of Laurentia. Lithosphere, p.L580-1.
Ferri, F., Rees, C., Nelson, J., and Legun, A., 1999, Geology and Mineral Deposits of the Northern Kechika Trough between Gataga River and the 60th Parallel: Geological Survey Branch, Mineral Resources Division, British Columbia Ministry of Energy and Mines Bulletin 107, 122 p.
Coats, R.P. and Preiss, W.V., 1980. Stratigraphic and geochronological reinterpretation of late Proterozoic glaciogenic sequences in the Kimberley region, Western Australia. Precambrian Research, 13(2-3), pp.181-208.
Condon, D., Zhu, M., Bowring, S., Wang, W., Yang, A. and Jin, Y., 2005, U-Pb ages from the neoproterozoic Doushantuo Formation, China: Science, v. 308, no. 5718, p.95-98.

Diehl, J.F. and Haig, T.D., 1994. A paleomagnetic study of the lava flows within the Copper Harbor Conglomerate, Michigan: new results and implications. Canadian Journal of Earth Sciences, 31(2), pp.369-380.
Dirks, P.H. and Wilson, C.J., 1990. The geological evolution of the Reynolds Range, central Australia: evidence for three distinct structural-metamorphic cycles. Journal of Structural Geology, 12(5-6), pp.651-665.
Dunlop, D. J., and Buchan, K. L., 1977, Thermal remagnetization and the paleointensity record of metamorphic rocks: Physics of the Earth and Planetary Interiors, v. 13, no. 4, p. 325-331.
Kean, W.F., Williams, I., Chan, L., Feeney, J., 1997. Magnetism of the Keweenawan age Chengwatana lava flows, northwest Wisconsin. Geophysical Research Letters 24, 1523–1526.
Kent, D. V., and W. K. Witte (1993), Slow apparent polar wander for North America in the Late Triassic and large Colorado Plateau rotation, Tectonics, 12, 291–300, doi:10.1029/92TC01966.

Kent, D.V. and Irving, E., 2010. Influence of inclination error in sedimentary rocks on the Triassic and Jurassic apparent pole wander path for North America and implications for Cordilleran tectonics. Journal of Geophysical Research: Solid Earth, 115(B10).

Kodama, K.P. and Dekkers, M.J., 2004. Magnetic anisotropy as an aid to identifying CRM and DRM in red sedimentary rocks. Studia Geophysica et Geodaetica, 48(4), pp.747-766.

Liebes, E. and P. N. Shive, Magnetization acquisition in two Mesozoic red sandstones, Phys. Earth Planet. Int., v. 30, 396–404, 1982.

Marshak, S. and Paulsen, T., 1996, Midcontinent US fault and fold zones: A legacy of Proterozoic intracratonic extensional tectonism?. Geology, v. 24, no. 2, p.151-154.

Marshak, S., Domrois, S., Abert, C., Larson, T., Pavlis, G., Hamburger, M., Yang, X., Gilbert, H. and Chen, C., 2017, The basement revealed: Tectonic insight from a digital elevation model of the Great Unconformity, USA cratonic platform. Geology, v. 45, no. 5, p.391-394.

Marshak, S., Karlstrom, K. and Timmons, J.M., 2000, Inversion of Proterozoic extensional faults: An explanation for the pattern of Laramide and Ancestral Rockies intracratonic deformation, United States. Geology, v. 28, no. 8, p.735-738.

Mattinson, J.M., 2005, Zircon U-Pb chemical abrasion ("CA-TIMS") method: combined annealing and multi-step partial dissolution analysis for improved precision and accuracy of zircon ages: Chemical Geology, v. 220, no. 1, p. 47-66.

Molina-Garza, R. S., J. W. Geissman, and R. Van der Voo (1995), Paleomagnetism of the Dockum Group (Upper Triassic), northwest Texas: Further evidence for the J1-cusp in the North America apparent polar wander path and implications for rate of Triassic apparent polar wander and Colorado plateau rotation, Tectonics, 14, 979 – 993, doi:10.1029/ 95TC01456.

Morra, G., Seton, M., Quevedo, L. and Müller, R.D., 2013. Organization of the tectonic plates in the last 200Myr. Earth and Planetary Science Letters, 373, pp.93-101.

Palmer, H. Paleomagnetism and correlation of some Middle Keweenawan rocks, Lake Superior. Canadian Journal of Earth Science 7, 1410–1436 (1970).

Palmer, H. C., and Hayatsu, A., 1975, Paleomagnetism and K-Ar dating of some Franklin lavas and diabases, Victoria Island: Canadian Journal of Earth Sciences, v. 12, no. 8, p. 1439-1447.

Palmer, H. C., Baragar, W. R. A., Fortier, M., and Foster, J. H., 1983, Paleomagnetism of Late Proterozoic rocks, Victoria Island, Northwest Territories, Canada: Canadian Journal of Earth Sciences, v. 20, no. 9, p. 1456-1469.

Porter, S. M. and Knoll, A. H., 2000, Testate amoebae in the Neoproterozoic Era: evidence from vase-shaped microfossils in the Chuar Group, Grand Canyon: Paleobiology, v. 26, p. 360–385.

Porter, S.M., Meisterfeld, R. and Knoll, A.H., 2003. Vase-shaped microfossils from the Neoproterozoic Chuar Group, Grand Canyon: a classification guided by modern testate amoebae. Journal of Paleontology, 77(3), pp.409-429.

Powell, C.McA., Li, Z.X., McElhinny, M.W., Meert, J.G., Park, J.K., 1993. Paleomagnetic constraints on timing of the Neoproterozoic breakup of Rodinia and the Cambrian formation of Gondwana. Geology 21, 889–892.

Powell, C.McA., Preiss, W.V., Gatehouse, C.G., Krapez, B., Li, Z.X., 1994. South Australian record of a Rodinian epi- continental basin and its mid-Neoproterozoic breakup (~700 Ma) to form the palaeo-Pacific Ocean. Tectonophy- sics 237, 113–140.

Rooney, A. D., Macdonald, F. A., Strauss, J. V., Dudás, F. Ö., Hallmann, C., and Selby, D., 2014, Re-Os geochronology and coupled Os-Sr isotope constraints on the Sturtian snowball Earth: Proceedings of the National Academy of Sciences, v. 111, no. 1, p. 51-56.

Rooney, A.D., Strauss, J.V., Brandon, A.D., and Macdonald, F.A., 2015, A Cryogenian chronology: Two long-lasting, synchronous Neoproterozoic glaciations: Geology, v. 43, no. 5, p. 459-462

Ross, G.M., Bloch, J.D., Krouse, H.R., 1995, Neoproterozoic strata of the southern Canadian Cordillera and the isotopic evolution of seawater sulfate: Precambrian Research, v. 78, p. 70–99.

Rowley, D. B., and Lottes, A. L. (1988). Plate-kinematic reconstructions of the North Atlantic and Arctic: Late Jurassic to present. Tectonophysics, 155(1), 73-120.

Schlische, R.W., 1995, Geometry and origin of fault-related folds in extensional settings: AAPG bulletin, v. 79, no. 11, p.1661-1678.

Schlische, R.W., 2003, Progress in understanding the structural geology, basin evolution, and tectonic history of the eastern North American rift system: The Great Rift Valleys of Pangea in Eastern North America, v. 1, p. 21-64.

Schmidt, Phillip W., George E. Williams, and Michael O. McWilliams. "Palaeomagnetism and magnetic anisotropy of late Neoproterozoic strata, South Australia: Implications for the palaeolatitude of late Cryogenian glaciation, cap carbonate and the Ediacaran System." Precambrian Research 174, no. 1 (2009): 35-52.

Seton, M., Müller, R.D., Zahirovic, S., Gaina, C., Torsvik, T., Shephard, G., Talsma, A., Gurnis, M., Turner, M., Maus, S. and Chandler, M., 2012. Global continental and ocean basin reconstructions since 200Ma. Earth-Science Reviews, 113(3), pp.212-270.

Sharp, I.R., Gawthorpe, R.L., Armstrong, B. and Underhill, J.R., 2000, Propagation history and passive rotation of mesoscale normal faults: implications for synrift stratigraphic development: Basin Research, v. 12, no. 3-4, p. 285-305

Shipilov, E.V., 2008. Generations of spreading basins and stages of breakdown of Wegener's Pangea in the geodynamic evolution of the Arctic Ocean. Geotectonics, 42(2), pp.105-124.

Smith, M.D., Arnaud, E., Arnott, R.W.C. and Ross, G.M., 2011, The record of Neoproterozoic glaciations in the Windermere Supergroup, southern Canadian Cordillera: Geological Society, London, Memoirs, v. 36, no. 1, p.413-424.

Steiner, M. B. (2003), A cratonic Middle Jurassic paleopole: Callovian- Oxfordian stillstand (J-2 cusp), rotation of the Colorado Plateau, and Jurassic North American apparent polar wander, Tectonics, 22(3), 1020, doi:10.1029/2001TC001284.

Steiner, M. B., and S. G. Lucas (2000), Paleomagnetism of the Late Triassic Petrified Forest Formation, Chinle Group, western United States: Further evidence of ''large'' rotation of the Colorado Plateau, J. Geophys. Res., 105, 25,791–25,808, doi:10.1029/2000JB900093.

Stokking, L. B., and Tauxe, L., 1990, Properties of chemical remanence in synthetic hematite: testing theoretical predictions: Journal of Geophysical Research: Solid Earth (1978–2012), 95(B8), p. 12639-12652.

Strauss, J.V., Roots, C.F., Macdonald, F.A., Halverson, G.P., Eyster, A.E., and Colpron, M., 2014b. Geological map of the Coal Creek Inlier, Ogilvie Mountains (NTS 116B/10-15 and 116C/9,16) (1:100,000 scale), Yukon Geological Survey, Open File 2014-XX.

Swanson-Hysell, N.L., Maloof, A.C., Weiss, B.P. and Evans, D.A., 2009. Nature Geoscience, 2(10), pp.713-717.

Sweeney, J.F., Weber, J.R. and Blasco, S.M., 1982. Continental ridges in the Arctic Ocean: LOREX constraints. Tectonophysics, 89(1-3), pp.217-237.

Tan, X. and Kodama, K.P., 2002. Magnetic anisotropy and paleomagnetic inclination shallowing in red beds: Evidence from the Mississippian Mauch Chunk Formation, Pennsylvania. Journal of Geophysical Research: Solid Earth, 107(B11).

Tan, Xiaodong, Kenneth P. Kodama, Stuart Gilder, and Vincent Courtillot. "Rock magnetic evidence for inclination shallowing in the Passaic Formation red beds from the Newark basin and a systematic bias of the Late Triassic apparent polar wander path for North America." Earth and Planetary Science Letters 254, no. 3 (2007): 345-357.

Tauxe, L., N. Kylstra, *and* C. Constable *(*1991*),* Bootstrap statistics for paleomagnetic data*,* J. Geophys. Res.*, 96(*B7*),* 11723–11740*, doi:*10.1029/91JB00572.

Tauxe, L., and D. V. Kent (1984), Properties of a detrital remanence carried by haematite from study of modern river deposits and laboratory rede- position experiments, Geophys. J. R. Astron. Soc., 77, 543–561.

Thorkelson, D. J., 2000, Geology and mineral occurrences of the Slats Creek, Fairchild Lake and "Dolores Creek" areas, Wernecke Mountains (106D/16, 106C/13, 106C/14), Yukon Territory. Exploration and Geological Services Division, Yukon, Indian and Northern Affairs Canada, Bulletin 10, 73p.

Thorkelson, D., Abbott, J., Mortensen, J., Creaser, R., Villeneuve, M., McNicoll, V., and Layer, P., 2005, Early and Middle Proterozoic evolution of Yukon, Canada: Canadian Journal of Earth Sciences, v. 42, no. 6, p. 1045–1071, doi: 10.1139/E05-075.

Timmons, J. Michael, Karl E. Karlstrom, Matthew T. Heizler, Samuel A. Bowring, George E. Gehrels, and Laura J. Crossey. 2005, Tectonic inferences from the ca. 1255–1100 Ma Unkar Group and Nankoweap Formation, Grand Canyon: Intracratonic deformation and basin formation during protracted Grenville orogenesis." Geological Society of America Bulletin 117, no. 11-12: 1573-1595.

Torsvik, T.H., Tucker, R.D., Ashwal, L.D., Eide, E.A., Rakotosolofo, N.A., de Wit, M.J., 1998, Late Cretaceous magmatism in Madagascar: palaeomagnetic evidence for a stationary Marion hotspot. Earth Planet. Sci. Lett. v. 164, p. 221 – 232.

Trompette, R., 1997, Neoproterozoic ~ 600 Ma aggregation of Western Gondwana: a tentative scenario. Precambrian Research, v. 82, no.1-2 , p.101-112.

Veevers, J.J., Walter, M.R., Scheibner, E., 1997. Neoproterozoic tectonics of Australia–Antarctica and Laurentia and the 560 Ma birth of the Pacific Ocean reflect the 400 m.y. Pangean Supercycle. J. Geol. 107, 225–242.

Wendt, I. and Carl, C., 1991, The statistical distribution of the mean squared weighted deviation. Chemical Geology: Isotope Geoscience Section, v. 86, no. 4, p.275-285.

Werner R, Schmincke HU, Sigvaldason G., 1996, A new model for the evolution of table mountains: volcanological and petrological evidence from Herðubreið and Herðubreiðartogl volcanoes (Iceland): Geol Rundschau v. 85, p. 390-397.

Whitmeyer, S.J. and Karlstrom, K.E., 2007, Tectonic model for the Proterozoic growth of North America. Geosphere, v. 3, no. 4 , p.220-259.

Wingate, M.T., Pisarevsky, S.A. and Evans, D.A., 2002. Rodinia connections between Australia and Laurentia: no SWEAT, no AUSWUS?. Terra Nova, 14(2), pp.121-128.

Woodcock, N.H. and Fischer, M., 1986, Strike-slip duplexes. Journal of structural geology, v. 8, no.7 , p.725-735.

Yonkee, W. A., Dehler, C. D., Link, P. K., Balgord, E. A., Keeley, J. A., Hayes, D. S., Wells, M. L., Fanning, C. M., and Johnston, S.M., 2014, Tectono-stratigraphic framework of Neoproterozoic to Cambrian strata, west-central US: Protracted rifting, glaciation, and evolution of the North American Cordilleran margin: Earth-Science Reviews, v. 136, p. 59-95.

Zartman, R.E., Nicholson, S.W., Cannon, W.F. and Morey, G., 1997. U–Th–Pb zircon ages of some Keweenawan Supergroup rocks from the south shore of Lake Superior. Canadian Journal of Earth Sciences, 34(4), pp.549-561.

TABLE S1. SAMPLING LOCATIONS WITH DETAILS OF LATITUDE, LONGITUDE, BEDDING, FORMATION & MEMBER

Latitude (°N)	Longitude (°W)	Locality	Bedding S/D (°)	Location	Formation	Member
36.264	111.882	A1301-matrix	225/3	Nankoweap Butte	Sixtymile Fm.	N.A.
36.268	111.885	A1302	120/9	Nankoweap Butte	Kwagunt Fm.	Walcott
36.268	111.886	A1303	133/39	Nankoweap Butte-E. limb of syncline	Kwagunt Fm.	Carbon Butte
36.268	111.886	A1304	140/39	Nankoweap Butte-E. limb of syncline	Kwagunt Fm.	Awatabi
36.274	111.886	A1305	157/33	Nankoweap Butte-E. limb of syncline	Kwagunt Fm.	Carbon Butte
36.276	111.890	A1306	70/22	Nankoweap Butte-Center of syncline	Kwagunt Fm.	Carbon Butte
36.274	111.890	A1307	65/24	Nankoweap Butte-W. limb of syncline	Kwagunt Fm.	Awatabi
36.274	111.890	A1308	64/31	Nankoweap Butte-W. limb of syncline	Kwagunt Fm.	Carbon Butte
36.274	111.891	A1309	44/29	Nankoweap Butte-W. limb of syncline	Kwagunt Fm.	Carbon Butte
36.167	111.839	A1310	304/12	Carbon Butte-center of syncline	Kwagunt Fm.	Carbon Butte

Latitude—locality Latitude (degrees north)
Longitude—locality longitude (degrees west)
Locality—number of locality sampled in study
Bedding S/D—strike and dip orientation of bedding
Location—broad regional location, see Figure 2.
Formation, Member—details on stratigraphic unit sampled

TABLE S2. SAMPLE LEAST SQUARE FITS AND UNBLOCKING RANGES

Sample	*Type of fit	&Component	Geographic coordinates		Tilt-corrected coordinates		Unblocking Range	*MAD*##	#Arc			
			D (°)	*I* (°)	*D* (°)	*I* (°)	(G or °C)	(°)	(°)			
A1301-1A	L	LT	262.4	-7.8	262.8	-6.4	NRM-300	13.2				
A1301-1A	L	HT	307.8	36.4	308.1	33.4	650-680	11.2				
A1301-1B	L	HT	291.6	-1.1	291.6	1.4	635-670	4.9				
A1301-2A	C	Ht.	338.2	-40.9	337.7	-37.9	680-690	1.6	21.7	264.6	22.5	265.
A1301-2A	L	HTs	356.1	58.3	358.7	60.8	NRM-675	3.8				
A1301-2B	L	LT	227.1	-2.6	227.3	-3.1	NRM-100	10.8				
A1301-2B	L	HT	288.2	24.2	287.3	26.5	660-680	9.6				
A1301-2B	L	HTs	5.7	62.8	9.7	65	200-660	8				
A1301-3A	L	LT	48.3	59.2	53.3	59.5	NRM-200	8				
A1301-3A	C	HT	354.7	-1.8	354.7	0.9	670-680	3.5	76.9	285.9	101.7	252.
A1301-3A	L	HTs	73.3	71.9	81.7	70.8	575-675	3.1				
A1301-3B	L	HTs	351.1	61.3	353.7	64	NRM-570	4.6				
A1301-3B	L	HT	281.7	37.1	282.9	34.6	575-705	2.9				
A1301-4A	L	LT	318.3	-22.2	318.5	-19.2	NRM-100	9.9				
A1301-4A	L	HT	268.6	-3.8	268.7	-2.3	450-705	5				
A1301-4B	L	LT	308.9	-20	309.1	-17.1	NRM-100	6.4				
A1301-4B	L	HT	276.1	-8	275.8	-10.3	450-705	1.6				
A1302-1A	L	LT	249.2	24.8	247	17.7	NRM-100	1.6				
A1302-1A	L	MT	281.8	73.4	259.1	68.7	200-400	14.1				
A1302-1B	L	LT	282.1	19	279.4	16	NRM-AF125	4.1				
A1302-1B	L	MT	304.4	46.7	294.8	46.6	AF150-400	12.2				
A1302-1B	C	HT	9	-19	9.8	-10.5	AF150-400	12.1	82.2	249.9	79	246.
A1302-2A	L	LT	278.7	17.9	276.3	14.4	NRM-AF125	2.8				
A1302-2A	L	MT	307.3	63	289.6	62.8	100-450	7.1				
A1302-2A	C	HT	11.9	-21.2	12.5	-12.7	375-450	10.9	92.8	259.3	90	256.
A1302-2B	L	LT	290.2	20.5	287	18.8	NRM-AF15	3.2				
A1302-2B	L	MT	306	52.6	294.2	52.6	AF150-400	11.1				
A1302-2B	C	HT	18	-22.1	18.7	-13.3	300-450	13.4	97.4	253.8	95.4	251.
A1303-1A	L	LT	152.6	-3.1	146.7	-14	NRM-350	8.9				
A1303-1A	L	MT	31.4	49.3	321.3	81.7	400-540	10.3				
A1303-1A	C	HT	35.9	13.8	31.2	52.2	530-545	6.9	-13.3	237.3	-5	245.
A1303-2A	L	LT	78	35.8	115.1	61.5	NRM-AF125	6.2				
A1303-2A$	L	MT	65.4	3.3	71.8	39	200-565	14.2				
A1303-2A	L	HT	120.5	-29.5	105.1	-14.7	590-650	5.7				
A1303-2B	L	LT	95.5	34	129.6	49.6	NRM-200	13.9				
A1303-2B	L	HT	109.9	-35.6	94	-14	530-680	9.1				
A1303-2C$	L	LT	0.5	0.9	354.2	26.8	NRM-200	45.4				
A1303-2C$	L	HT	91.7	-17.4	89.8	9.9	300-575	18.8				
A1303-2C	L	HT	108.3	-36.9	92.1	-14.4	570-635	8.8				
A1303-3A$	L	LT	359.2	62.7	271.2	63.5	NRM-300	31.8				
A1303-3A**$	L	HT	86.1	-28.2	80.2	2.6	350-560	13.8				
A1303-3A**	L	HT	104.3	-25.6	95.8	-3.1	575-635	10.4				
A1303-3B$	L	LT	172.9	80.5	213.6	44.7	NRM-100	23.9				

A1303-3B**$	L	HT	103.4	-11.7	102.6	9.1	200-570	14.6				
A1303-3B**	L	HT	95.9	-31.8	86.1	-4.5	605-680	12.9				
A1304-1A	L	MT	19.7	71.4	253.3	65.9	NRM-375	2.9				
A1304-1A	C	HT	73.2	23.8	91.5	57.2	540-560	5.3	-79.9	127.3	-106.7	100.
A1304-1B	L	MT	21.1	56.5	291.8	72.4	NRM-400	3.1				
A1304-1B	L	HT	123.6	-40.6	101.8	-22	400-570	14.7				
A1304-2A	L	LT	319.1	69.7	260.6	46.9	NRM-AF150	6.4				
A1304-2A	L	MT	14.1	57.6	289.1	68.5	100-375	9.8				
A1304-2A	L	HT	129.6	-50.3	97.7	-32	500-605	14.2				
A1304-2B	L	MT	14.5	59.3	284.4	68.6	NRM-350	9.7				
A1304-2B	L	HT	122.2	-42	100	-22.4	500-590	6.3				
A1305-1A	L	LT	196.9	27	203.7	3.9	NRM-AF75	5				
A1305-1A	L	HT	287.6	51.2	273.3	23.2	450-690	14.6				
A1305-1B	L	LT	182.4	40.7	199.7	21.6	NRM-AF50	11.2				
A1305-1B$	L	HT	296.1	70.5	266.9	42.2	560-670	32.5				
A1305-3A$	no fits with *MAD* <15°											
A1305-3B	L	MT	345.6	63.4	292.7	51.8	NRM-560	11.7				
A1305-3B††	L	HTs	358.3	56.9	307.2	54.2	650-695	6.2				
A1305-4A	L	MT	326	54.5	293.8	38.5	LN2-375	13.3				
A1305-4A	L	HT	298.7	53.4	279.1	28.2	670-690	13.6				
A1305-4B	L	MT	296.9	65.7	270.7	38.4	AF50-400	14.1				
A1305-4B	L	HT	275.9	54.8	264.8	24.2	580-680	5.2				
A1306-1A$	L	MT	104.8	20.6	109.2	7.3	100-450	28.8				
A1306-1A	L	HT	104.9	10.2	106.1	-2.8	450-660	13.2				
A1306-1B$	L	MT	262.2	57.9	227.8	55.8	NRM-400	19.6				
A1306-1B	L	HTs	333.1	66	284.3	86.6	450-660	5.3				
A1306-2A$	L	HTs	325.5	17.8	322.1	39	NRM-450	11.2				
A1306-2A	L	HTs	358.3	53.8	20.6	73.4	560-700	11.9				
A1306-2B**	L	MT	350.4	27.1	354.0	48.6	NRM-565	2.2				
A1306-2B**	L	HTs	351.2	45.4	0.3	66.7	660-700	7.5				
A1307-1A	L	LT	329.4	43.8	323.1	67.4	NRM-AF150	7.3				
A1307-1A†	L	MT	305.9	68.6	220.1	78.1	200-400	8.4				
A1307-1A†	C	HT	8.1	-23.5	5	2.7	100-300	9.9	81.4	235.3	81.5	287.
A1307-1B	L	LT	31.5	43.3	56.8	52.7	NRM-AF150	7.7				
A1307-1B†	L	MT	314.3	78.7	173.8	75.9	100-350	4.1				
A1307-1B†	C	HT	9	-5.2	10.2	15	100-450	8.1	-155.4	274.5	-37.8	252.
A1307-2A	L	LT	6	43.5	26.8	62.3	NRM-100	2.2				
A1307-2A†	L	MT	27.4	58.5	72.9	65.9	200-375	11.7				
A1307-2A†	C	HT	348.6	-24.9	347.2	5.1	200-375	6.5	-169.2	330.4	-18.6	201.
A1307-2B	L	LT	351.9	68.1	93	83.6	NRM-100	3.8				
A1307-2B†	L	MT	18.6	69.6	111.1	68.4	100-350	3.4				
A1307-2B	L	HT	111.2	-11.9	101.5	-33.4	375-450	5.7				
A1307-3A†	L	MT	295.8	55.4	255.4	68.1	AF100-350	5.3				
A1307-3A†	C	HT	352.6	-18.5	351.8	4.5	100-545	9.4	167.1	267.5	6.4	265.
A1307-3B$	L	MT	210.5	22.6	205.4	7.5	NRM-300	7.3				
A1309-1A	L	HTs	30.3	58.7	75.9	54.3	NRM-605	14.7				
A1309-1B	L	LT	190.2	-63.4	254.9	-65	NRM-300	17				
A1309-1B	L	HTs	340.4	19	349.4	44.4	475-680	14.1				

A1309-2A	L	HTs	10.4	55.3	59.1	61.3	100-680	5.8				
A1309-2B	L	MT	68.8	71.3	108	50	AF25-350	13.8				
A1309-2B	L	HTs	30.2	42.2	57.7	42.9	400-660	6.9				
A1309-3A	L	LT	40.5	1.7	41.9	3.8	AF25-350	7.3				
A1309-3A	L	HTs	341.2	33.7	358.6	58	620-660	5.8				
A1309-3B	L	HTs	341.9	45.4	12.3	68	200-675	5.2				
A1310-1	L	LT	274.6	16	278.2	21.5	NRM-100	14.2				
A1310-1[$]	L	MT	52.1	-3.5	52.7	-15	300- 560	23.9				
A1310-1	C	HT	250.6	67.9	279.3	75.7	560-660	7.9	121.6	268.3	91.4	238.
A1310-2A[$]	L	LT	100.9	48.7	90.6	43	AF25-350	25.1				
A1310-2A	L	HT	102.4	-20.3	107	-24.3	300-665	7.8				
A1310-2B[$]	L	LT	15.1	11.8	15.6	0.7	NRM-250	24.6				
A1310-2B	L	HT	88.8	-8.8	90.9	-15.6	300-665	8.3				
A1310-3A[$]	L	MT	83.6	11	82.4	3.2	400-570	15.3				
A1310-3A	L	HT	98.6	-27.6	105	-32.2	550-660	14.4				
A1310-3B[$]	L	MT	129.6	-8.3	131.2	-6.9	300-650	15.5				
A1310-3B	L	HT	106.2	-10.7	108.7	-14.1	565-660	5.7				

HT Locality Means:

locality	*D*	*I*	*D*	*I*	*k*	*MAD/* α_{95}	n_{sample}
A1303	108.5	-32.4	95	-10.8	86.4	7.7	6
A1304	122.4	-47.4	96.2	-26.6	48.1	15.1	4
A1305	287.5	53.5	272.3	25.3	89.9	10.7	3
A1306	104.9	10.2	106.1	-2.8	N.A	13.2	1
A1307	102.3	-19.3	89.6	-35.1	46.4	18.3	5
A1310	99.8	-13.2	102.9	-17.8	24.2	17.2	5

MEANS	***D/I*** (°)	***k***	α_{95} (°)	***D/I*** (°)	***k***	α_{95} (°)	**Pass/Fail: unfolding range**	**Pole Latitude/ Longitude (°N/°E)**	A_{95} (°)	***N***	***K***
Mean of averaged localities	106.6/-26.25	11.2	20.9	97.3/-19.8	38.4	10.9	Pass: 54 – 109% unfolding	11.9/162.5	7.5	6	81.7
Mean of averaged strata within 15 cm of each other[$$]	108.5/-29.6	13.9	13.4	98.7/-19.8	52.3	6.7	Pass: 70 – 109% unfolding	13.1/161.5	4.6	10	111.

*L=linear C=great circle

[&]Component designation used for analysis, LT=low temperature, MT=mid temperature, HTs=steep high temperature, HT=shallow high temperature

[#]rake within the plane of the farthest point and the antipode of the beginning point- bound the arc within the plane where the primary direction may lie (both geographic and stratigraphic).

[$]sample excluded from subsequent analysis

**HT component unblocking temperatures consistent with magnetization carried by minerals with two distinct unblocking temperatures. Lower unblocking temperature directions are shallower.

[##]*MAD*=maximum angle of deviation

[†]A1307 samples-overlap of demagnetization temperatures for linear fit MT and great circle fit HT components

[††] A1305-3B displays HTs

Note: all A1308 samples and A1305-3A: no fits with MAD <15°

[$$]Pole when these directions are combined with the Carbon Butte-Awatabi sites of Weil et al. (2004): $Pole_{Longitude}$=163.2°E, $Pole_{Latitude}$=14.3°N, A_{95}=3.7°, K=100.9, N=16

TABLE S3. IRM ACQUISITION PARAMETERS

Sample	Field where 99.5% sIRM is reached (mT)	Component 1			Component 2		
		% Contribution	$B_{1/2}$ (mT)	*dp*	% Contribution	$B_{1/2}$ (mT)	*dp*
A1303-2Ay	2200	100.00	502.09	0.26			
A1303-3By	1600	100.00	485.79	0.27			
A1310-2Ax	2600	100.00	676.10	0.32			
A1310-3Bx	2600	100.00	708.23	0.27			
A1304-1By	2600	94.40	631.00	0.26	5.60	63.10	0.35
A1304-2Ax	2400	85.78	617.90	0.26	14.22	62.43	0.27
A1305-4Ay	2200	79.00	631.00	0.41	21.00	50.10	0.42
A1305-3By	2600	42.30	489.80	0.22	57.70	141.30	0.55
A1309-1Ax	2400	69.80	398.10	0.50	30.20	79.40	0.50
A1309-1By	2600	67.40	446.70	0.40	32.60	63.10	0.40
A1309-2Ay	2600	75.30	588.80	0.34	24.70	72.40	0.40

TABLE S4. BACKFIELD AND HYSTERESIS PARAMETERS

	*B_{cr} Coercivity of remanence (mT)	*M_r Saturation remanence (Am^2)	†M_s Saturation magnetization (Am^2)	†M_r Saturation remanence (Am^2)	†B_c Coercive Field (mT)	†M_r/†M_s (squareness)	B_{cr}/B_c
A1303-2Ay	563.6	3.8E-06	1.5E-06	8.8E-07	300.60	0.58	1.88
A1303-3By	520.4	3.0E-06	3.0E-07	1.7E-07	300.10	0.56	1.73
A1310-2Ax	719.3	1.4E-05	2.3E-06	1.3E-06	310.70	0.57	2.31
A1310-3Bx	733.6	1.0E-05	1.2E-06	7.7E-07	413.60	0.62	1.77
A1304-1By	628.5	1.9E-06	3.5E-07	2.5E-07	323.10	0.71	1.95
A1304-2Ax	533.8	4.9E-07	1.2E-07	6.9E-08	69.37	0.56	7.70
A1305-4Ay	392.9	3.7E-06	9.5E-07	4.4E-07	82.92	0.46	4.74
A1305-3By	294.71	7.9E-07	8.4E-07	2.2E-07	50.00	0.27	5.89
A1309-1Ax	203.03	8.2E-06	2.9E-06	1.2E-06	56.84	0.41	3.57
A1309-1By	221.00	4.3E-06	6.0E-07	1.9E-07	37.05	0.31	5.96
A1309-2Ay	396.16	2.3E-06	6.4E-07	2.1E-07	53.67	0.32	7.38

*from IRM backfield experiments
†from hysteresis experiments

TABLE S5. MEMBER DATA FROM WEIL ET Al. 2004

Member and Site	*D/I* (in situ) (°)	*D/I* (tilt corrected)(°)	α_{95} (°)	*k*	*n/N*
Walcott:					
JG60-18	290/54	303/29	18	27	7/7
JG60-6	299/50	290/30	13	28	7/7
Walcott HT Mean†	*D/I* = 294.70/52.09 α_{95} = 14.92 *k* = 281.93	*D/I* = 296.37/29.88 α_{95} = 24.31 *k* = 107.65	tilt α_{95} >> in situ α_{95}		2 sites 14 samples
Awatabi:					
JG-53-2	107/-31	98/-13	11	76	6/7
Carbon Butte					
#AW-13-4	272/3	272/23	9	39	8/8
AW-12-10	88/−25	94/−34	12	65	6/8
AW-12-11	103/−13	108/−28	16	258	6/8
**AW-12-13*	*85/−28*	*83/−36*	*21*	*20*	*7/8*
AW-12-14A	92/−20	97/−39	12	60	6/8
AW-12-14B	97/−19	103/−37	12	39	8/8
Carbon Butte HT Mean†	*D/I* = 94.48/-16.08 α_{95} = 9.57 *k* = 64.89	*D/I* = 98.66/-32.65 α_{95} = 8.49 *k* = 82.05	Indeterminate 95% confidence bounds: -10–109% unfolding		5 sites 32 samples
Awatabi + Carbon Butte HT Mean†	*D/I* = 96.38/-18.63 α_{95} = 9.86 *k* = 47.10	*D/I* = 98.53/-29.38 α_{95} = 9.44 *k* = 51.31	Indeterminate 95% confidence bounds: -10–109% unfolding		6 sites 38 samples
Carbon Canyon					
AW-12-8	260/60	256/17	13	27	6/8
AW-12-9	256/48	254/−11	9	90	7/8
AW-12-15	**277/31**	**285/35**	**15**	**24**	**7/8**
AW-12-19	**299/−8**	**296/1**	**16**	**16**	**7/7**
AW-12-20	**284/5**	**285/7**	**7**	**53**	**6/7**
AW-13-1	264/6	264/−5	11	31	7/7
AW-13-2	264/18	259/10	15	16	7/7
AW-13-3	254/26	245/22	14	21	7/8
AW-13-6	241/−20	247/−5	12	31	7/8
AW-13-7	260/−19	263/2	17	22	6/7
AW-13-8	267/−2	267/10	14	24	7/7
AW-13-9	252/−29	259/−7	15	27	6/7
AW-13-10	264/−6	263/13	14	25	7/7
AW-13-11	263/−30	269/−5	19	13	7/8
Carbon Canyon HT Mean†	*D/I* = 265.14/5.34 α_{95} = 16.14 *k* = 7.03	*D/I* = 264.93/6.11 α_{95} = 9.65 *k* = 17.93	Pass fold test 95% confidence bounds: 72 – 109% unfolding		14 sites 94 samples
Jupiter					
AW-12-22	268/−11	266/−5	16	20	8/8
AW-12-23	270/3	272/5	6	112	8/8
PDF- Carbon Butte					
T-52-1	5/64	313.26/68.78	8	56	8/8
T-65-1	4/54	21.64/44.07	11	50	5/8
T-65-2	5/53	21.86/42.92	7	107	6/8
JG-60-2	0/61	325.62/44.00	6	122	6/8
JG-60-3	5/55	319.23/34.68	8	151	6/8
JG-53-4	13/57	320.21/63.65	10	51	6/8
JG-53-5	345/63	295.92/54.84	10	30	9/9
AW-13-5	6/51	36.16/60.33	7.8	61	8/8
AW-12-12	11/68	35.25/50.65	9	61	8/8

D and *I*—mean declination and inclination
k—Fisher's (1953) precision parameter
α_{95}—radius of confidence circle for the mean direction
n/N—number of samples used/total number of samples
#reversed for calculations of means
*discarded from subsequent analysis because α_{95} >20°
†Mean calculated from sites with α_{95}<20°: first column = in situ mean, second column=tilt corrected mean, third column= fold test result and 95% confidence bounds, fourth column=number of sites and samples

TABLE S6. POTENTIAL EXPLANATIONS FOR WALCOTT SITE MEANS

Explanation 1: varying the temperature steps used in line fits

Temperature steps used(°C)		Resultant *D*/*I* from linear least squares fit			
		D (°)	I (°)	MAD (°)	n_{steps}
HT	1: 685, 690, 695, 700	281.5	34.4	1.5	4
	2: 660, 695, 700	285.9	39.5	0.9	3
	3: 650, 695, 700	297.2	43.2	1.9	3
	4: 620,695, 700	291.7	48.9	6.6	3
	5: 580, 605, 690, 700	302.4	48.5	6.8	4
	6: 580, 605, 690	314.0	53.2	2.7	3
MT		351.1	61.3	4.6	29

Explanation 2: Mixing between samples with HT and HTs directions

Random directions drawn from HTs dataset κ: 27, *N*: 8, Mean *D*: 351, Mean *I:* 6

sample	D (°)	I (°)
HTs 1	336.8	52.7
HTs 2	292.1	75.1
HTs 3	310.1	56.7
HTs 4	304.3	61.4
HTs 5	358.9	49.9
HTs 6	336.4	73.0
HTs 7	3.4	52.2
HTs 8	359.7	62.3

Random directions drawn from HT dataset κ: 27, *N*: 8, Mean *D*: 281.5, Mean *I*: 34.3

sample	D (°)	I (°)
HT 1	296.3	29.5
HT 2	299.6	34.5
HT 3	278.0	44.5
HT 4	270.7	42.8
HT 5	291.6	12.9
HT 6	283.4	25.6
HT 7	290.6	43.0
HT 8	287.4	23.4

Computed site means with percentage of HT and HTs varying

	D (°)	*I* (°)	α_{95} (°)	*N* samples	*k*
0% HTs	287.67	32.34	9.45	8	35.33
12.5% HTs	290.72	36.11	15.99	8	17.32
25% HTs	289.49	41.15	16.75	8	11.89
50% HTs	297.14	45.00	17.4	8	11.88
75% HTs	312.38	57.25	15.95	8	13.01
100% HTs	336.98	62.69	10.99	8	26.36

D and *I*—mean declination and inclination
MAD—maximum angle of deviation
k—Fisher's (1953) precision parameter
α_{95}—radius of confidence circle for the mean direction
n_{steps}—number of steps used in least squares fit
N—total number

TABLE S7. REANALYZED A_R DATA FROM DATED SILL (PARK 1981)

Site	Paleomagnetic Pole			
	Latitude	Longitude	A_{95}	*N*
2	3	143		7
3	2	137		1
4	8	138		6
5	-2	139		4
13	2	141		6
#VGP mean	2.6	139.6	4.1	5

Site—Name of paleomagnetic site of Park 1981
Paleomagnetic pole—Latitude (^{o}N), Longitude (^{o}E), A_{95} (^{o}) = cone of 95% confidence and N = number of specimens for the sites, and overall number of sites for the VGP mean
#K=353.5 for this VGP mean

TABLE S8. HOTTAH SHEETS (PARK ET AL.1995)

Site	*n*	*D* (°)	*I* (°)	α_{95} (°)	*k*	Paleomagnetic pole		
						Latitude	Longitude	A_{95}
Gunbarrel Sheet*	**7**	**281**	**3**	**6**	**95**	**5.9**	**142.4**	**ND**
Calder Sheet Site 4†	**6**	**292**	**27**	**10**	**36**	**22.0**	**138.4**	**ND**
Calder Sheet Site 5§	4	307	24	26	7	26.1	123.4	ND
Margaret Sheet Site 6#	4	283	12	9	101	11.1	143.7	ND
Margaret Sheet Site 7**	4	278	20	8	80	12.7	150.4	ND
Margaret Sheet Mean	**ND**	**ND**	**ND**	**ND**	**ND**	**11.9**	**147.0**	**14.76**
Hottah Mean pole††	**ND**	**ND**	**ND**	**ND**	**ND**	13.3	142.7	14.0

Site—site name
n—number of samples
D and *I*—declination and inclination
α_{95}—radius of confidence circle for the mean direction
k—Fisher's (1953) precision parameter
*Pole calculated for site location 65.67N 118.14W
†Pole calculated for site location 65.53N 117.30W
§Site not included due to high α_{95}
#Poles calculated for site location 64.40N 117.13W
**Poles calculated for site location 64.50N 116.90W
††Pole calculated as mean of VGPs of Gunbarrel Sheet, Calder Sheet Site 4 and Margaret Sheet Mean

TABLE S9. LAURENTIAN PALEOMAGNETIC POLES FROM THE MACKENZIE MOUNTAINS SUPERGROUP

Unit/Fm Pole	Age (Ma)	Type of Age and Reference	Paleomagnetic Pole			Paleomagnetic Reference	NOTES
			Lat.	Long.	A_{95}		
Redstone river (RRF)	>732 Ma	Re-Os 732 Ma in overlying Coppercap	22	151	9	Park and Jefferson, 1991	Declinations and inclinations are affected by tectonic rotations and faulting
Thundercloud (TH)	740-750	correlations	1	150	21	Park and Jefferson, 1991	Large error due to tectonic rotation on declinations
Rusty Shale (LRA)	>811-820	811 Ma U-Pb zircon age from correlative Fifteenmile Group (Macdonald et al., 2010)	-8	133	17	Park and Jefferson, 1991	
Basinal Little Dal (bLD)	820-830	Correlations	-15	141	3	Park 1981	
Mudcracked (M)	830-840	Correlations	-9	143	8.5	Park 1984	
Katherine Group (K)	840-850	Correlations	9	150	5.7	Park and Aitken 1986a	
Tsozotene Fm (TA)	850-860	correlations	12	146	8	Park and Aitken 1986b	

A_{95}— radius of the circle of 95% confidence about the mean from Fisher statistics on site mean poles. If not available, $A_{95} \sim \sqrt{dp \times dm}$. dp and dm =semi-axes of the 95% ellipse of confidence about the mean (Khramov, 1987, p. 97).

TABLE S10. UINTA MOUNTAIN GROUP PALEOMAGNETIC DATA FROM BRESSLER (1981)

Site	*n*	*D* (°)	*I* (°)	α_{95} (°)	*k*	Paleomagnetic pole			corrected for flattening[§]		#Paleomagnetic pole	
						Latitude (°)	Longitude (°)	A_{95} (°)	*D* (°)	*I* (°)	Longitude (°)	Latitude (°)
Site 6-Hades Pass (upper part of Qtz) Western Uinta Mountains	8	106.3	22.1	15.9	13.0	4.6	140.1	12.2	106.3	28.8	318.1	-1.8
Site 5-Hades Pass (lower part of Qtz) Western Uinta Mountains	48	267.2	-15.3	1.3	241.9	-7.2	155	1.0	267.2	-20.3	154.1	-9.0
Site 5 overprint-Hades Pass (lower part of Qtz) Western Uinta Mountains	6	93.6	-24.4	10.5	41.8	11	167	8.2	93.6	-31.6	351.1	-13.8
Site 4-Mount Watson Western Uinta Mountains	7	278.6	-3.8	26	6.3	5.3	152	18.4	278.6	6.1	152.7	4.8
Site 3-Shale Moosehorn lake Western Uinta Mountains	14	269.8	-13.1	4.4	83.5	4.5	154.2	3.2	269.8	-5.1	153.6	-6.0
Site 2-Lower-Middle part of Uinta Mountain Group	13	274	0.1	9.6	19.8	3.1	158.3	6.8	274	-17.5	157.7	3.1
Site 1a and 1b-Lower part of Uinta Mountain Group	26	267.8	-3.3	8.6	11.9	-2.7	161.1	6.1	267.8	0.1	160.0	-3.1

Site—site name
n—number of samples
D and *I*—declination and inclination
α_{95}—radius of confidence circle for the mean direction
k—Fisher's (1953) precision parameter
Paleomagnetic pole—Latitude (°N), Longitude (°E), A_{95} (°) = cone of 95% confidence-used for final Uinta Mountain group mean calculations
[§]Inclination corrected for flattening using *f=0.738*
#Paleomagnetic Pole calculated using D and I corrected for inclination flattening

TABLE S11. UINTA MOUNTAIN GROUP PALEOMAGNETIC DATA WEIL ET AL. 2006

Locality and Site	Bedding		In situ				tilt corrected			[§]optional directions corrected for inclination flattening
	Strike(°)	Dip(°)	D(°)	I(°)	α_{95}(°)	k	D(°)	I(°)	D(°)	[§]I(°)
Sheep Creek Canyon										
SC 2	325	81	104.5	36	11.5	45	97.9	-25.3	97.9	-32.6
SC 5	324	80	102.6	58.7	12.7	53	77.4	-11	77.4	-14.8
SC 6	325	78	114	31.3	12.6	23.8	105.7	-18.8	105.7	-24.8
SC 9	293	43	97.5	-8.2	17.1	52.9	107.2	-16.5	107.2	-21.9
SC 10	301	55	81.2	33.3	11.9	108.4	71.3	-7.1	71.3	-9.6
SC 11	296	39	98.1	-12.5	4.1	115	110	-20.9	110	-27.4
SC 12	297	36	95.3	6.5	5.3	69.2	95.5	-7.1	95.5	-9.6
SC 13	286	38	88.7	15.6	6.5	1502	83	2	83	2.7
SC 13	286	38	82.3	32.9	12.5	98.1	68	12.7	68	17.0
SC 14	301	39	105.3	6.4	3.4	718.1	104.7	-4.7	104.7	-6.4
SC 15	298	30	108	6.4	11.6	63.8	106.2	0.6	106.2	0.8
SC 16	315	41	105.9	6	9.5	65.6	108.5	-13.8	108.5	-18.4
SC 17	308	41	90.5	10.2	7.5	48.1	91.9	-15	91.9	-20.0
SC 19	303	40	96.2	11.7	9.6	64.6	94.8	-7.4	94.8	-10.0
SC 20	304	35	97.4	6	5.7	64.6	98.5	-9.8	98.5	-13.2
SC 21	305	52	273.1	62.9	20.7	36.5	0	47.5	0	55.9
SC 22	287	30	90.8	22.3	6.4	39.3	82.1	11.5	82.1	15.4
SC 23	287	30	98.3	0.5	7.5	56	99.2	-3.9	99.2	-5.3
SC 24	267	20	95.1	-1.2	3.6	665.2	95	1.6	95	2.2
SC 26	257	22	89.8	-0.4	5.9	55.9	89	4.4	89	6.0
SC 71	294	33	99.5	-1.8	11.3	47.2	102.7	-9.4	102.7	-12.6
SC 72	318	25	96.4	18.4	15.9	24	93.2	1.1	93.2	1.5
SC 75	294	39	89.6	0.1	13.2	22	94.5	-15	94.5	-20.0
SC 77	284	32	90.6	11.1	7.5	66.3	86.8	2.5	86.8	3.4
SC 80	296	27	86.6	20.7	10.2	36	81	6.1	81	8.2
SC 83	284	30	103.3	-11.1	2.5	502.2	109	-9.9	109	-13.3
SC 84	278	95	90.9	-0.9	7.3	70.1	99.5	-7	99.5	-9.4
SC 85	280	30	77.2	17.9	8.2	46.4	71.7	4.7	71.7	6.4
SC 86	267	23	88.5	9.9	8.3	53.5	84.5	9.7	84.5	13.0
SC 87	279	35	89.6	-11.8	7.3	69.4	98.2	-15	98.2	-20.0
SC 88	292	27	74.3	10.7	11.6	44.3	73.4	-6.2	73.4	-8.4
SC 89	247	15	99.3	-19.5	11	23	102.7	-11.1	102.7	-14.9
SC 90	247	15	91.1	-21.8	9.6	50.1	95.6	-15.1	95.6	-20.1
Browne Lake										
BL 54[c]	278	5	–	–	–	–	–	–	–	–
BL 55[a]	278	5	41.7	57.9	6.4	114.9	37.8	53.7	37.8	61.5
BL 56	277	11	82.9	-5.8	13.1	35.1	84.3	-8.3	84.3	-11.2
Carter Creek										
CC 57	285	12	263.2	-13.4	5.8	–	261	-8.7	261	-11.7
CC 58	232	10	266.4	-6.7	4.4	–	265	-12.3	265	-16.5
CC 59	277	9	270.4	-11.8	12.9	–	268.6	-10.6	268.6	-14.2
CC 60	300	5	272	-5	3.4	–	271.7	-2.6	271.7	-3.5
CC 61	281	1	263.9	-5.9	11.7	–	263.8	-5.6	263.8	-7.6
Dowd Springs non-fold test rocks										
DS 29	–	0	98.7	-20.1	30.7	4.8	98.7	-20.1	98.7	-26.4
DS 29	–	0	281.1	-42.2	14.3	30.3	281.1	-42.2	281.1	-50.9
DS 30	107	4	290.9	-72.2	8.1	69.2	302.9	-71.5	302.9	-76.1
DS 31	217	3	107.1	3.3	20.6	8.2	107	6.1	107	8.2
DS 32	–	0	282	-36.1	24	11.1	282	-36.1	282	-44.7
DS 33	132	7	97	-14.7	19.9	39.5	95.7	-10.6	95.7	-14.2
DS 34	132	7	101.9	-5	10.8	23.7	101.6	-1.5	101.6	-2.0
DS 35	99	4	103.8	-7.2	8.8	31.1	103.3	-7.5	103.3	-10.1
DS 36	102	6	108.7	-23	9.3	31.4	106.1	-23.6	106.1	-30.6
DS 37	120	10	107.6	6.6	12.4	18.3	108.9	8.6	108.9	11.6
DS 38	102	12	91.7	-12.7	10.7	13.7	89.3	-10.3	89.3	-13.8
Dowd Springs fold test rocks										
DS 39	63	19	261.7	-0.2	11.5	48.33	260.8	11.5	260.8	15.4
DS 40	63	19	257.8	-38.7	12.7	64.1	270.5	12.7	270.5	17.0
DS 41	63	19	261.2	-19.4	8.5	139.59	266.3	8.5	266.3	11.4
DS 42	221	14	271.2	-0.6	14.8	46.69	270.3	14.8	270.3	19.7
DS 43	221	14	276.4	8.2	12.2	32.1	276.7	12.2	276.7	16.3
DS 44	221	14	271.4	-6.8	7.9	103.9	269.4	7.9	269.4	10.6
Flaming Gorge Section										
FG-AW-01	236	18	270.8	-9.3	16.5	57	267	-19	267	-25.0
FG-AW-02	236	18	264.4	-10.5	9.4	51.4	260	-18	260	-23.8
FG-AW-03	236	18	274	-7.6	11.8	110.2	271	-19	271	-25.0
FG-AW-04	236	18	255.6	4.6	11.4	35.4	257	-1	257	-1.4
FG-GA-01	232	15	264.9	-5.3	6.6	135.2	261	-18	261	-23.8
FG-GA-02	220	20	268.4	-1	20.1	15.5	266	-16	266	-21.2
FG-GA-03	229	17	266.5	-3.4	13.3	34	265	-13	265	-17.4
FG-GA-04[c]	205	17	262.2	7.8	10.4	54.7	262	-6	262	-8.1
FG-GA-05	236	16	–	–	–	–	–	–	–	–
FG-GA-06	238	18	275.1	0.9	9.1	72	274	-10	274	-13.4
FG-GA-07	237	18	271.1	-3.1	8.3	65.7	269	-13	269	-17.4
FG-GA-08	237	18	259.1	-3	6.7	101.8	257	-10	257	-13.4
FG 48	250	18	275.2	-8.2	4.4	–	271.7	-15.4	271.7	-20.5
FG 49[a]	273	18	267.7	-5.7	8.1	–	266.2	-3.8	266.2	-5.1

FG 50	254	20	295.3	-10.3	8.9	–	290.6	-23	290.6	-29.9
FG 51	268	16	275.1	-3.1	3.2	–	274	-4.9	274	-6.6
FG 52	268	18	279.2	-12.1	8.3	–	274.9	-15	274.9	-20.0
FG 53	296	15	275.5	2.5	7.5	–	276.8	7.6	276.8	10.2
Bull Canyon										
BC 01	29	13	270.6	5.9	6	101.1	267.9	8.8	267.9	11.8
BC 02[b]	55	16	280.2	6.2	16.6	13.9	277.2	7.3	277.2	9.8
BC 03[b]	16	19	267.3	-5.9	14.4	23.4	267	12.1	267	16.2
BC 04	51	20	276.4	-2.2	20.5	8	271.8	1.2	271.8	1.6
BC 05	51	20	274.2	10	14.2	22.5	272.3	8.7	272.3	11.7
BC 06	51	20	269	5.1	5.8	71.9	264.9	12.1	264.9	16.2
BC 07	49	12	279.4	2.5	8.4	44.4	277.9	5.8	277.9	7.8
BC 08	89	17	282.9	2.3	9.2	37.7	281.8	6.2	281.8	8.4
BC 09[a]	19	12	2.1	56.7	4.4	121.3	20.1	58.2	20.1	65.4
BC 10[b]	99	2	267.1	8.2	17.9	14.5	269	10.5	269	14.1
Home Mountain Canyon										
UMG-GA-01	112	82	289.5	21.2	15.9	24.1	271	0	271	0.0
UMG-GA-02	116	52	284.3	34.7	14.1	19.2	261	12	261	16.1
UMG-GA-03	113	66	287.9	31.7	18.4	18.2	262	8	262	10.8
Sparks–Talamantes Creek										
SP 01[a]	306	58	105.2	22.1	6.5	63.5	96.3	-4.6	96.3	-6.2
SP 02	295	62	67.8	59.2	14.3	29.7	45.4	4.1	45.4	5.5
SP 03	313	70	92.1	30.5	11.9	42.3	87.2	-20.9	87.2	-27.4
SP 04	299	61	95.9	35.6	9.2	43.9	77.4	0.2	77.4	0.3
SP 05	315	63	88.8	34.6	11.6	23.7	81.3	-15.8	81.3	-21.0
SP 06	324	66	99.9	26	8.6	50.7	98.6	-23.1	98.6	-30.0
SP 07	299	61	104.2	31.6	14	43.9	84.6	3.7	84.6	5.0
SP 08	312	65	95.7	20	9.2	43.8	96.3	-21.1	96.3	-27.6

Locality and Site—Locality and site names
n—number of samples
D and *I*—declination and inclination
α_{95}—radius of confidence circle for the mean direction
k—Fisher's (1953) precision parameter
Paleomagnetic pole—Latitude (°N), Longitude (°E), A_{95} (°) = cone of 95% confidence
[§]Tilt corrected directions with inclination corrected for flattening using *f=0.738*

TABLE S12. MESOPROTEROZOIC PALEOMAGNETIC POLES

Pole	Age (Ma)	Type and Age Reference	Paleomagnetic Pole				Paleomagnetic Reference
			Latitude (°N)	Longitude (°E)	A_{95} (°)	*N*	
North Shore Volcanic Group (upper SW sequence)	1098.4 ± 1.9, 1096.6 ± 1.7	Pb-Pb weighted mean, Davis and Green, 1997	35.8	182.1	3.1	47	Tauxe and Kodama, 2009; mean calculated in Fairchild et al., 2017
Portage Lake Volcanics	1096.2 ± 1.8	U-Pb concordia intercept, Davis and Paces, 1990	27.1	182.0	2.2	97	Books, 1972; Hnat et al., 2006
Chengwatana Volcanics	1094.6 ± 2.1	Pb-Pb zircon, weighted mean, Zartman et al., 1997	30.9	186.1	4.9	8	Kean, et al. 1997
Schroeder-Lutsen basalts	<1091.61 ± 0.14	CA-ID-TIMS Fairchild et al., 2017	27.1	187.8	3.0	50	Tauxe and Kodama, 2009; Fairchild et al., 2017;
Lake Shore Traps	1085.57 ± 0.25	CA-ID-TIMS Fairchild et al., 2017	23.1	186.4	4.0	31	Kulakov et al., 2013
Michipicoten Island Fm	1084.35 ± 0.20, 1083.52 ± 0.23	CA-ID-TIMS Fairchild et al., 2017	17	174.7	4.4	23	Palmer and Davis, 1987; Fairchild et al., 2017
Nonesuch Formation	1078 ± 24	Re-Os Cumming et al., 2010	7.3	174.7	3.0	29	Henry et al., 1977; Symons et al., 2013
Bangemall Sills	1071±8, 1067±14, 1068±22, Mean: 1070 ± 6	U-Pb SHRIMP Baddeleyite/ zircon Wingate and Giddings, 2004	33.8	95.0	8.3	11	Wingate and Giddings, 2004
Cardenas Basalts-Unkar Intrusives	1080 ± 2,1080 ± 3 1088 ± 3,1094 ± 2	U-Pb baddeleyite Bright et al. 2014 on correlative units	32.0	185.0	9.6	16	Weil et al., 2003

Pole—Name of paleomagnetic pole
Age—Age of paleomagnetic pole
Type and Age reference—method used to obtain age and reference
Paleomagnetic pole—Latitude (°N), Longitude (°E), A_{95} (°) = cone of 95% confidence and N = number of sites
Paleomagnetic Reference—reference for paleomagnetic pole

1 Supplemental Figures

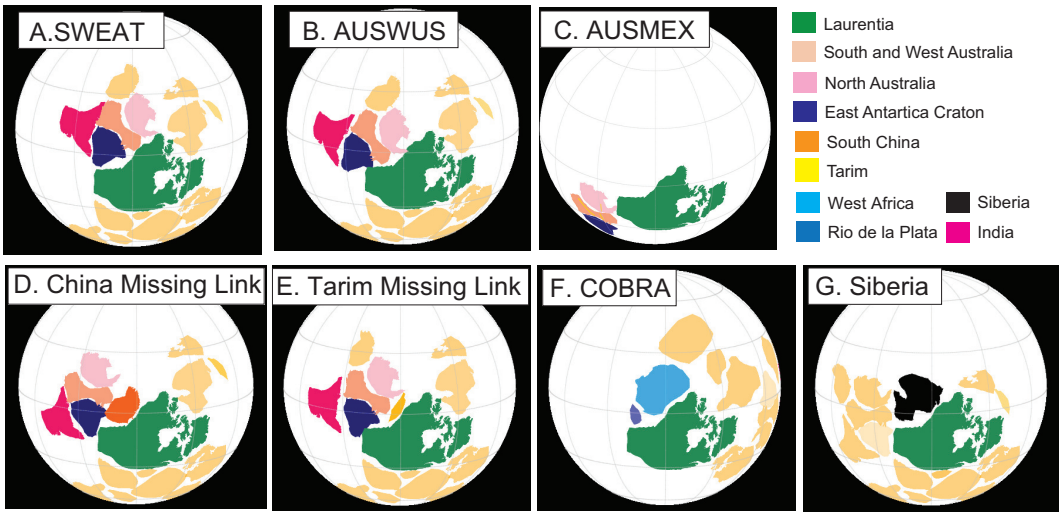

Figure S1: Rodinia reconstructions for the Western Laurentia margin. A. SWEAT (after Hoffman, 1991; Moores, 1991; and Daizal 1991). B. AUSWUS (after Karlstrom et al., 1999). C. AUSMEX (after Wingate and Giddings, 2004). D. Missing Link China (After Li et al., 2008). E. Missing Link Tarim (After Wen et al., 2016). F. COBRA (after Evans, 2009). G. Siberia (after Sears and Price 1978; 2003). Note that coloring is inconsistent between in order to highlight the different models of the conjugate margin to the western Laurentia margin.

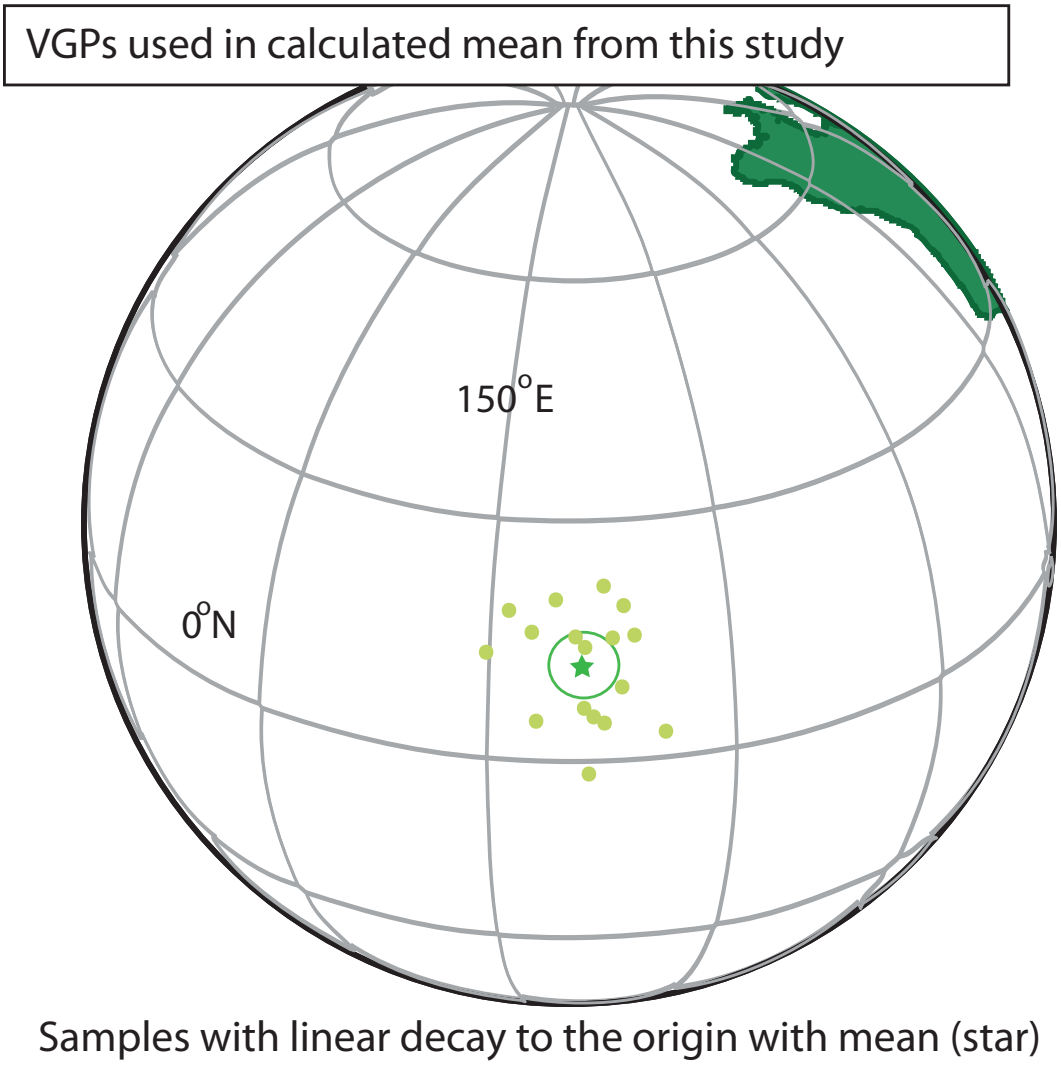

Figure S2: Paleomagnetic poles from samples that displayed HT components with linear decays to the origin and their overall mean.

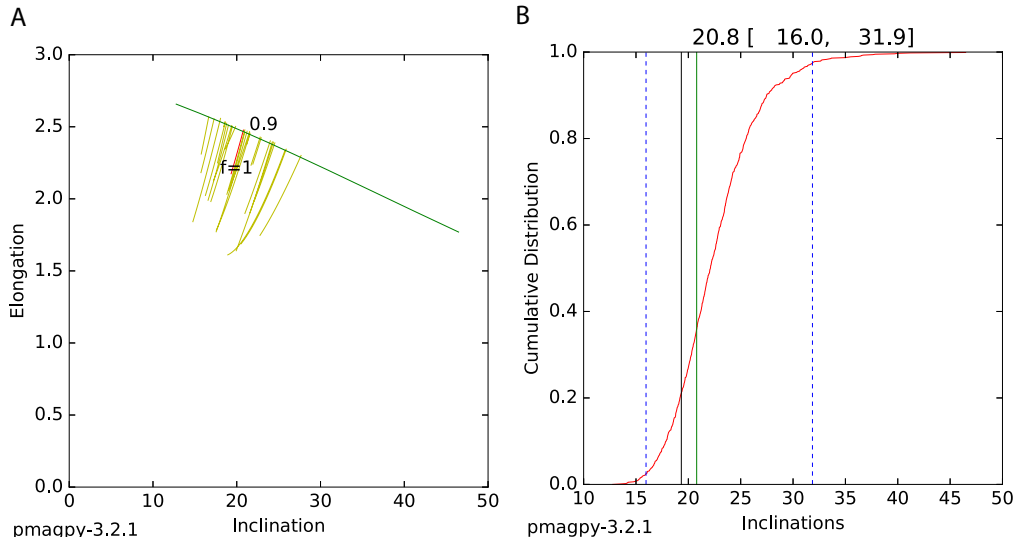

Figure S3: E-I inclination flattening for our Carbon Butte-Awatabi Dataset. A. Elongation/inclination pairs as a function of f, data plus 25 bootstrap samples. B. Cumulative distribution of bootstrapped optimal inclinations plus uncertainties. Estimate from original data set plotted as solid line.

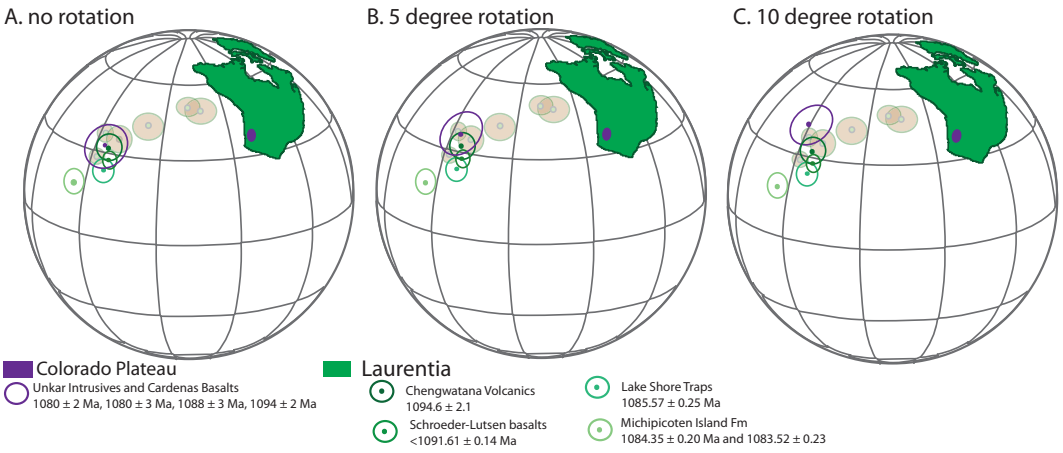

Figure S4: Testing the block rotation of the Colorado plateau by comparing the paleomagnetic poles from the ca. 1094-1080 Ma Grand Canyon Unkar intrusives and Cardenas basalts to the 1095 Ma-1083 Ma portions of the midcontinent rift Logan Loop. A, B, C. Colorado plateau rotated 0, 5, 10 respectively relative to North America using an Euler pole of 34.6N 254.6E (Hamilton, 1988).

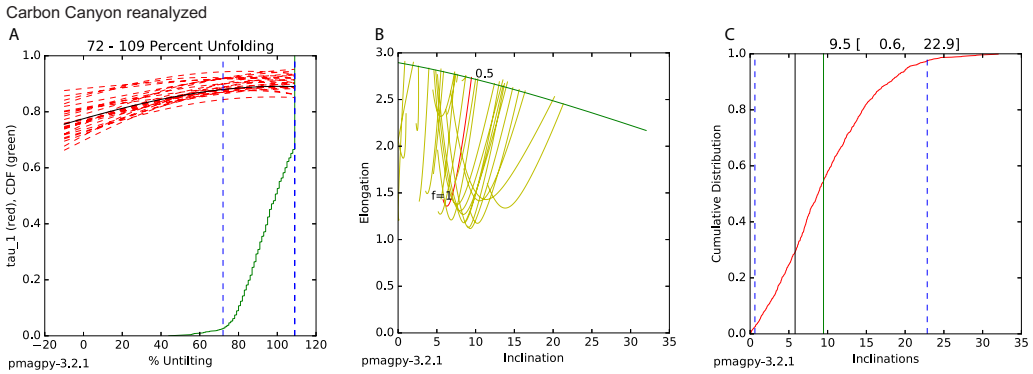

Figure S5: A. Fold test for reanalyzed Carbon Canyon sites (Weil et al., 2004). B. Elongation/inclination pairs as a function of f, data plus 25 bootstrap samples. C. Cumulative distribution of bootstrapped optimal inclinations plus uncertainties. Estimate from original data set plotted as solid line.

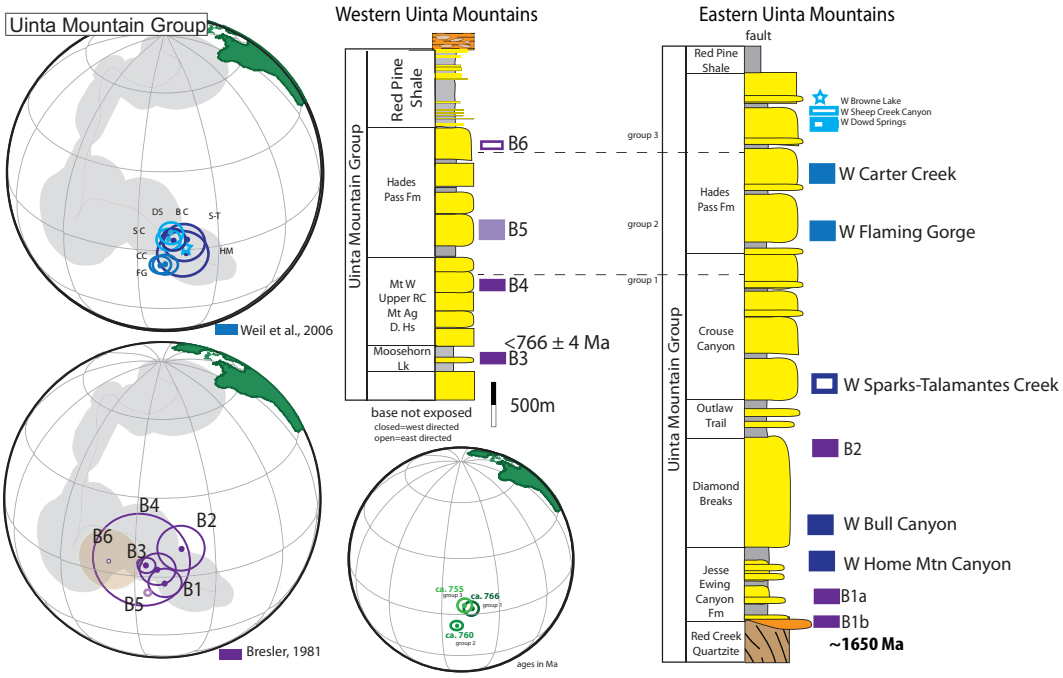

Figure S6: Uinta Mountain Group poles from Bressler (1981) and Weil et al. (2006). Reported and proposed sampling heights allowed separation of poles into three groupings that were used in subsequent analysis.

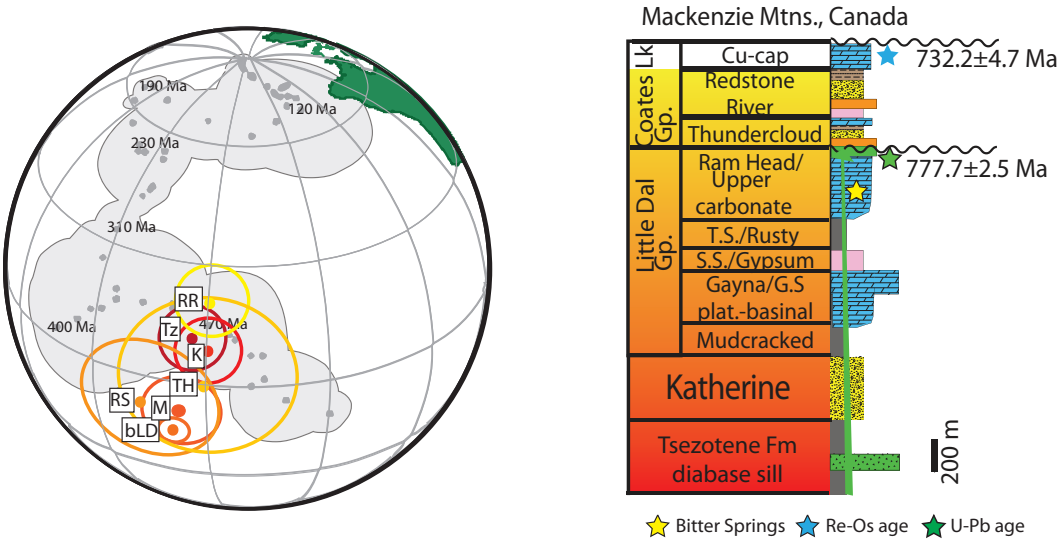

Figure S7: Mackenzie Mountains poles from Park and Jefferson (1991) and references therein.

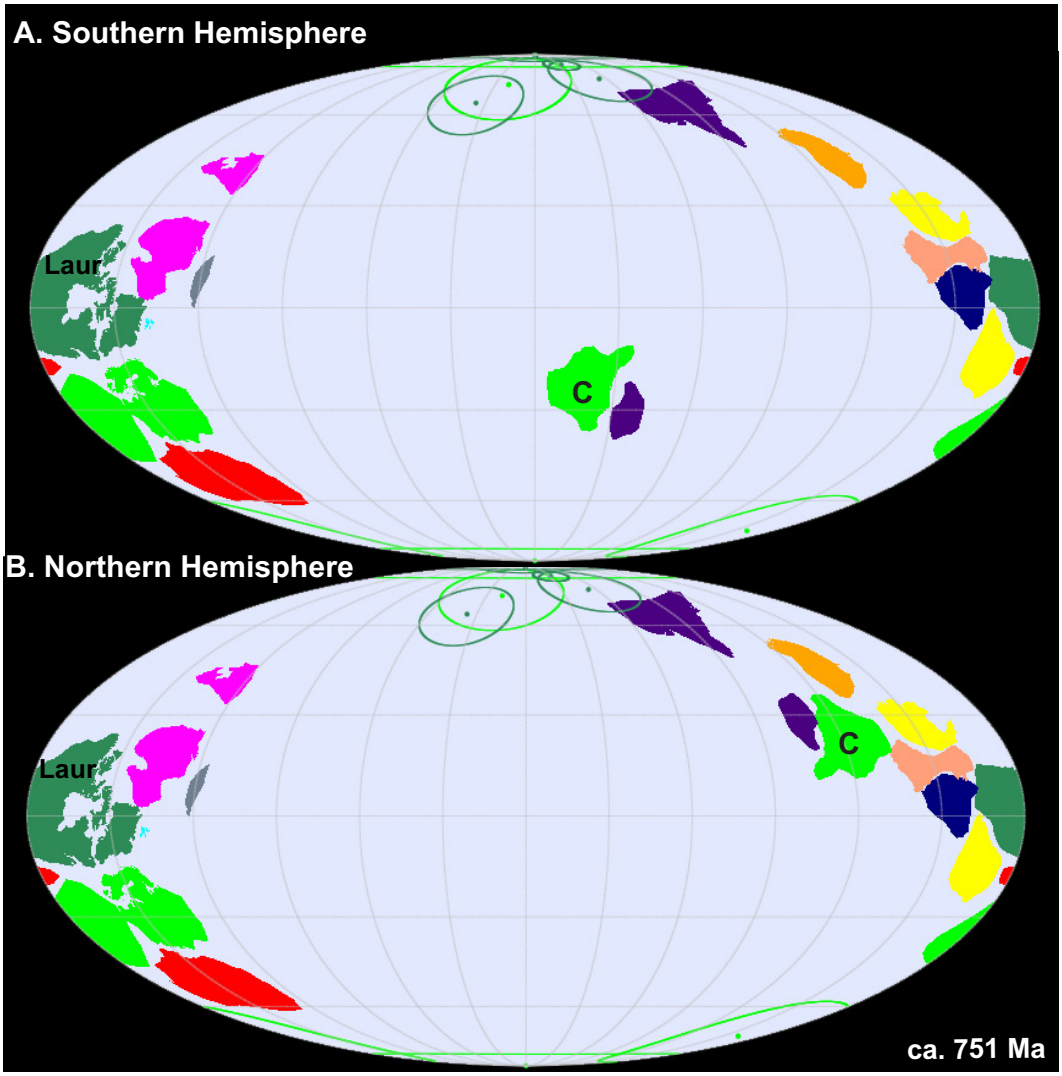

Figure S8: Figure S9. Comparison between reconstructions of Congo using both pole polarities. A. Congo in the southern hemisphere. B. Congo in the Northern Hemisphere.

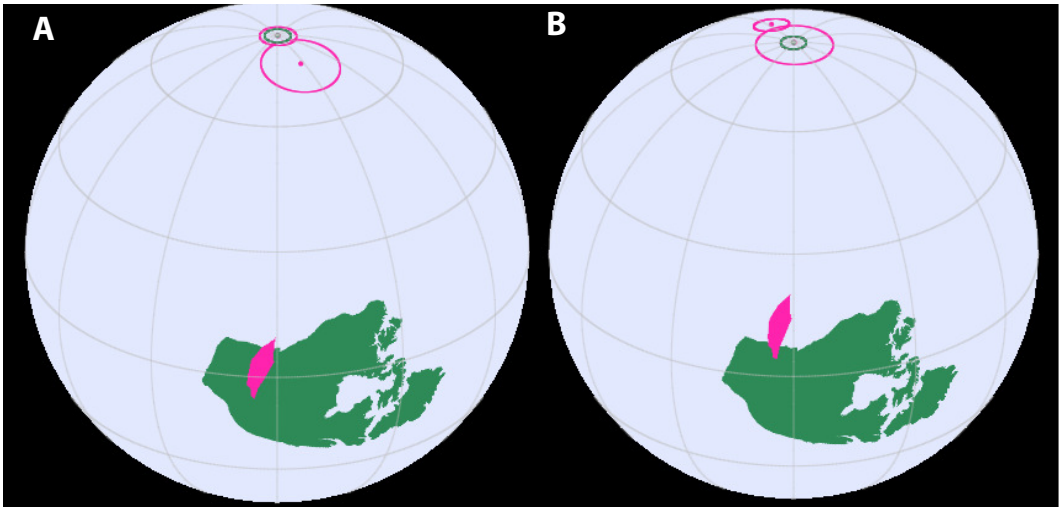

Figure S9: Comparison between reconstructions of Tarim using the Baiyisi pole (A), as well as both of the less-constrained Qiaoenbrak Formation pole (B).

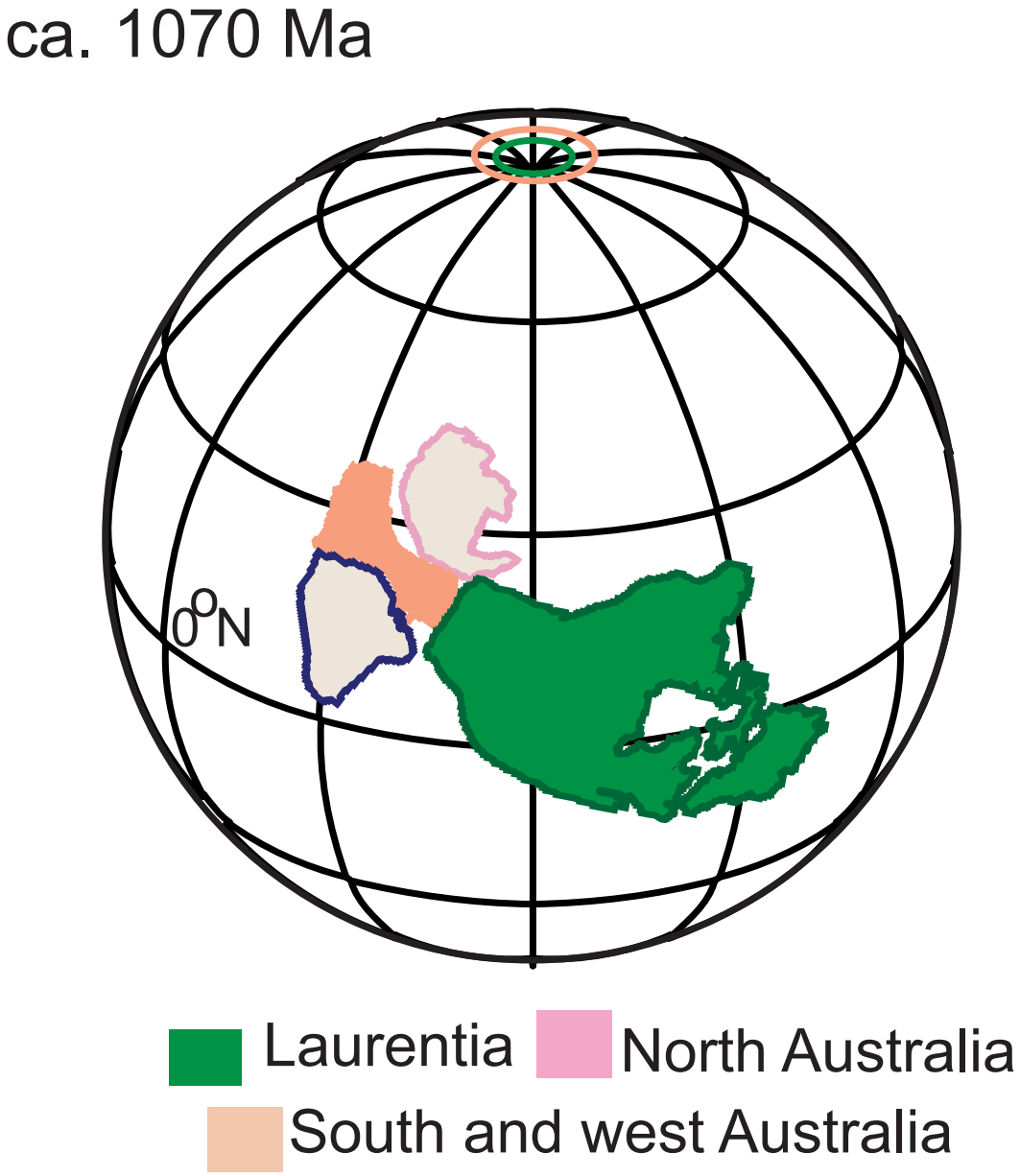

Figure S10: ca. 1070 Ma reconstruction with only Laurentia, Australia and associated cratons. Paleomagnetic poles are from the Australian Bangemall sills (1070 Ma U-Pb) and the Laurentian Nonesuch Shale (1087 Ma Re-Os).

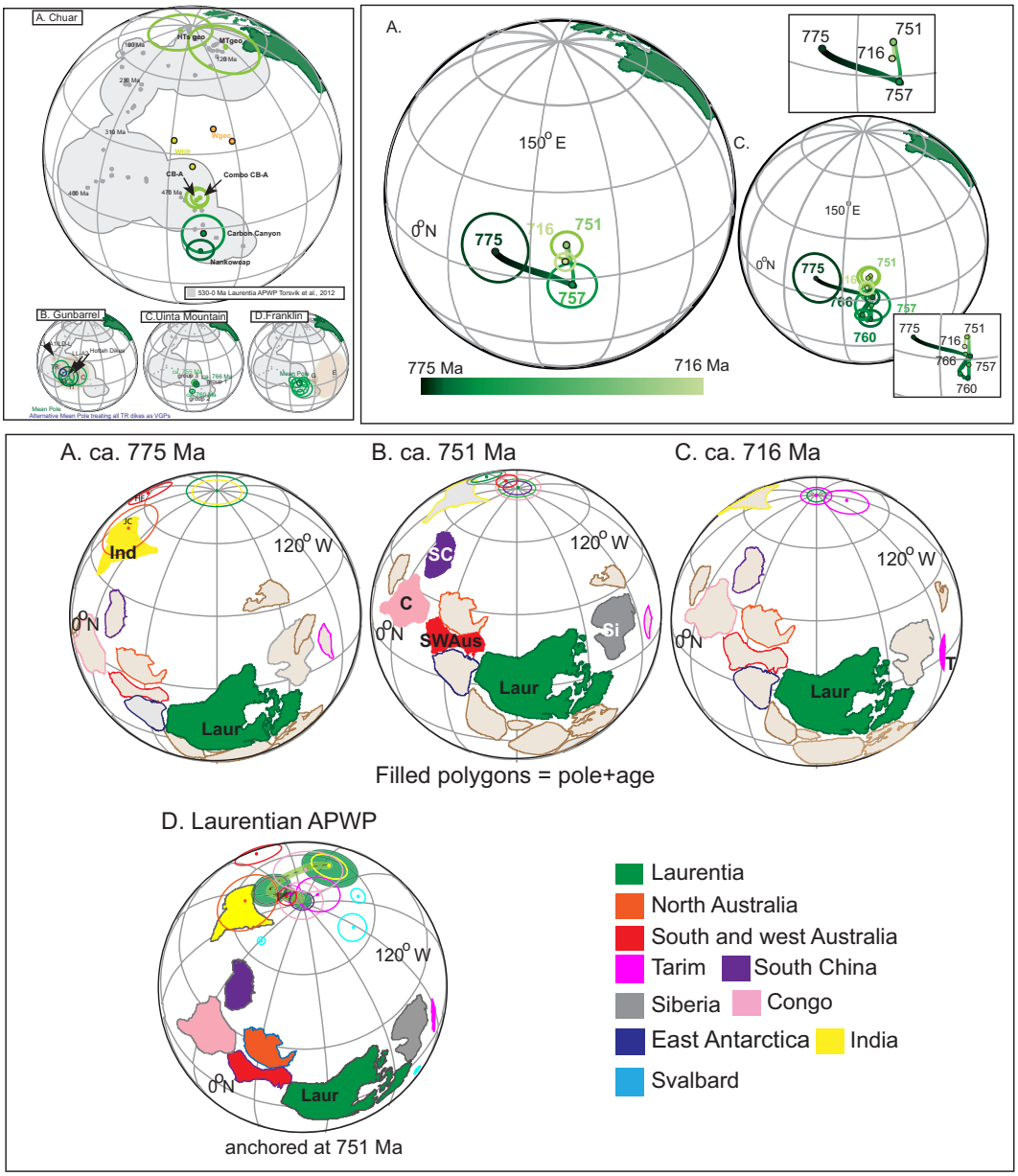

Figure S11: Figures similar to those in the manuscript, but for poles that are corrected for possible inclination flattening.